Journal of Colloid and Interface Science 705 (2026) 139477

Contents lists available at ScienceDirect

Journal of Colloid And Interface Science

journal homepage: www.elsevier.com/locate/jcis

Regular Article

Unveiling the methane hydrate–water interfacial free energy through direct molecular simulation at coexistence conditions

Iván M. Zerón [a], José Manuel Míguez [a], Jesús Algaba [a], Bruno Mendiboure [b], Felipe J. Blas [a,*]

[a] Laboratorio de Simulacion Molecular y Quimica Computacional, CIQSO-Centro de Investigacion en Quimica Sostenible and Departamento de Ciencias Integradas, Universidad de Huelva, 21007-Huelva, Spain

[b] Laboratoire des Fluides Complexes et Leurs Reservoirs, UMR5150, Universite de Pau et des Pays de l'Adour, B. P. 1155, Pau Cdex 64014, France

GRAPHICAL ABSTRACT

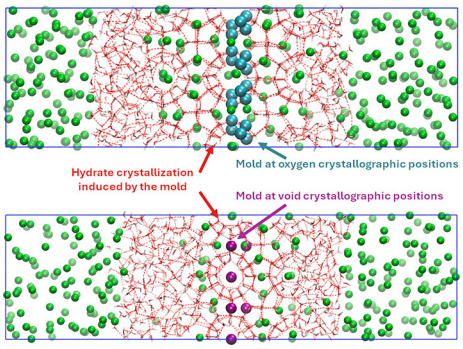

ARTICLE INFO

Keywords:
Interfacial free energy
Methane hydrate
Hydrate-water interface
Computer simulation

ABSTRACT

Hypothesis: The interfacial free energy between hydrate and water phases is a key thermodynamic parameter that governs both nucleation kinetics and crystal growth of gas hydrates. In these strategic materials—crystalline inclusion compounds where hydrogen-bonded water cages encapsulate small guest molecules such as methane (CH_4) and carbon dioxide (CO_2)—this interfacial energy plays a crucial role in determining phase stability and formation pathways. Given the significance of gas hydrates in energy storage, CO_2 sequestration, and climate-related processes, accurately determining their interfacial energies is essential for advancing both fundamental understanding and technological applications. Despite its importance, the hydrate–water interfacial energy remains poorly constrained due to substantial experimental uncertainties and the limitations of indirect estimation methods. For example, reported experimental values for CH_4 hydrate span a wide range from 28 to 40 mJ/m^2. Interestingly, some studies suggest these values are comparable to the interfacial free energy of the hexagonal ice (ice Ih)–water interface, approximately 32 mJ/m^2, hinting at potential analogies between clathrate hydrate and ice interfaces.

Calculations: In this work, we present a direct molecular simulation of the CH_4 hydrate–water interfacial free energy using two novel and independent extensions of the mold integration method. These extensions are specifically designed to induce the formation of a thin, planar hydrate–water interface and to compute the reversible work required to create it. For this purpose, we employ the TIP4P/Ice force field—one of the most reliable water models available—known for accurately reproducing the melting temperature of ice Ih under ambient conditions.

* Corresponding author.
E-mail address: felipe@uhu.es (F.J. Blas).

https://doi.org/10.1016/j.jcis.2025.139477
Received 1 August 2025; Received in revised form 12 November 2025; Accepted 12 November 2025

Available online 17 November 2025

Findigns: Our results show that the interfacial free energy of CH_4 hydrate is significantly higher than that of CO_2 hydrate, offering a natural explanation for their markedly different nucleation behaviors. This aligns with prior predictions based on Classical Nucleation Theory, as well as advanced sampling techniques such as Transition Path Sampling and Transition Interface Sampling. Notably, our computed value for CH_4 hydrate approaches $\sim 40\,mJ/m^2$, in agreement with the upper bound of existing experimental estimates, while values for CO_2 hydrate and ice Ih remain closer to $\sim 30\,mJ/m^2$. This direct, theory-independent determination provides new insights into the molecular mechanisms underlying hydrate formation and offers robust benchmarks for predictive modeling and the design of hydrate-based technologies.

1. Introduction

In the late 1700s, while investigating the solubility of newly discovered "airs" (gases), several natural philosophers observed the unexpected formation of ice-like solids –even at temperatures above the freezing point of water– when certain gases were bubbled through cold water or when such mixtures were frozen. Sir Humphry Davy, a pioneer of electrochemistry and mentor to Michael Faraday, later identified these substances as compounds formed by water and gas, coining the term "gas hydrates". After more than a century of continued study, these materials were ultimately recognized as clathrates: crystalline structures in which small guest molecules are trapped within a hydrogen-bonded lattice of water cages, as is the case for methane (CH_4) and carbon dioxide (CO_2) under suitable thermodynamic conditions [1–3].

Notably, clathrate structures have also been identified in intermetallic [4,5], in which metallic guest ions are encapsulated by frameworks of group 14 elements (Si, Ge, or Sn). More recently, clathrate-like architectures have been shown to self-assemble from colloidal particles [6,7], opening new possibilities for the formation of larger cages and enabling mesoscale phenomena with potential relevance to biological and photonic applications.

A key common point between traditional gas hydrates and more challenging and sophisticated clathrates is the host–guest interaction, which underpins their use in natural gas capture [1] and gas storage [8]. CH_4 hydrates, in particular, have garnered significant attention as an alternative energy resource due to their vast natural deposits [1,3,9–16]. Additionally, hydrates play a critical role in climate dynamics, as they represent a major reservoir of greenhouse gases that could be destabilized under changing environmental conditions [1,3,9,10,17–19]. Beyond energy and climate, gas hydrates are also being explored for their potential in CO_2 sequestration [20–22], as well as for gas storage [23] and transportation technologies [24–26].

A comprehensive understanding of the thermodynamic mechanisms governing hydrate nucleation and growth is essential for the effective exploitation of gas hydrates [1,3,27–52]. The simplest but also primary theoretical framework to understand homogeneous nucleation of hydrates is Classical Nucleation Theory (CNT) [27]. According to the CNT, two parameters mainly govern the nucleation process: the nucleation driving force and the interfacial free energy between the hydrate and water. An accurate knowledge of these two key properties is necessary for a comprehensive understanding of the mechanisms governing hydrate nucleation. Unfortunately, this is not an easy task. Although obtaining accurate values for the nucleation driving force is inherently challenging, reliable estimates can often be derived from indirect experimental observations and analyses [28]. Molecular simulations have become an invaluable tool for quantifying nucleation driving forces in both pure substances and hydrate-forming systems [50,51,53–56].

However, there is no universally accepted or standardized experimental method for determining solid–fluid interfacial free energies [57], in contrast to the well-established techniques available for fluid–fluid interfaces [58,59]. The proper description of properties at solid–liquid interfaces is a challenging task that requires careful theoretical and computational treatment. One of the reasons, among others, of the difficulties arises from the existence of two similar but different magnitudes of critical importance associated with interfaces. The work required to create a new surface and the work associated with stretching an existing surface. As mentioned, although similar, they may differ and it is important to distinguish between these two contributions.

Following this line of reasoning, Gibbs introduced two distinct interfacial quantities [60]: (1) the interfacial free energy, γ, defined as the reversible work needed to create a unit area of interface in a system without a pre-existing interface; and (2) the interfacial stress, $\hat{\mathbf{f}}$, which quantifies the excess stress in a system with an interface relative to the bulk. While the interfacial free energy is a scalar quantity, the interfacial stress is generally a two-dimensional, second-order tensor. In the special case of liquid–liquid or liquid–vapor interfaces, which possess rotational symmetry, the interfacial stress tensor reduces to a single scalar that is numerically equal to the interfacial free energy, i.e., $\gamma = f$.

Although Gibbs clearly distinguished between γ and $\hat{\mathbf{f}}$, the subsequent literature often employed the term "tension" when referring to γ, even in the context of solid interfaces. This shift in terminology has historically generated confusion, and in some instances has even led to claims that γ and f need not be considered as distinct interfacial properties. This issue is examined in detail by Di Pascuale and Davidchack [61], who revisit the classical Shuttleworth relation [62] from a molecular simulation perspective, and show that their results are in good agreement with the theoretical predictions across all cases studied. In line with their arguments, and also following Cahn [63], we recommend the use of the term surface stress to designate $\hat{\mathbf{f}}$, while reserving the term interfacial free energy for γ. The word tension should preferably be avoided, or used exclusively as a synonym for stress, since its meaning is more naturally associated with tensile forces acting at an interface rather than with the energetic cost of creating an interface. In this work, we deliberately avoid the term "surface tension" when referring to solid–liquid interfaces, and consistently use "interfacial free energy" instead.

One of the employed methods for estimating solid–liquid interfacial free energy is based on the classical Young's equation [64]. Solid–fluid interfacial free energies can also be estimated using the Gibbs–Thomson relation [65–67]. Uchida et al. [68,69] and Anderson et al. [70,71] independently reported interfacial free energies of $\gamma_{hw} = 39$, 34(6), and $32(3)\,mJ/m^2$ for CH_4 hydrate and 28(6) and $30(3)\,mJ/m^2$ for CO_2 hydrate using this technique, respectively. In all cases, uncertainties are large due to limitations of the methodology. Some publications indicate that these values closely match the interfacial free energy of the hexagonal ice (ice Ih)–water interface, approximately $32\,mJ/m^2$, suggesting analogous interfacial behavior between clathrate hydrates and ice [35,37,68–71]. However, new nucleation rate calculations of CH_4 and CO_2 hydrates published during the last five years indicate that this may not be the case [44,46,47,49–51,72–74]. This is a crucial topic that warrants thorough analysis, as γ_{hw} plays a pivotal role in determining hydrate nucleation and growth [1,3,27].

Computer simulations offer an interesting alternative way to predict solid-fluid interfacial free energies in cases where experiments are scarce. A comprehensive and up-to-date discussion of the most relevant computer simulation methodologies is presented in detail in a recent review article authored by some of us [75]. CNT [76–79], combined with

the Seeding approach [37,53,55], is the only indirect computational methodology reported in the literature for determining the interfacial free energies of hydrates.

Jacobson and Molinero performed the first indirect calculation of the CH_4 hydrate-water interfacial free energy [35]. They performed Seeding simulations of a slab of an M liquid (a single particle with properties intermediate between CH_4 and CO_2 [32]) in contact with a saturated water solution with M, containing clusters of M hydrates of different sizes to determine the melting temperatures of the crystalline nuclei. Combining these results with the well-known Gibbs-Thomson relationship [65–67], they obtained a value $\gamma_{hw} \approx 36(2)\,mJ/m^2$ that lies between the experimental value for the CO_2 hydrate-water interface and that for the CH_4 hydrate-water interfacial energy. One year later, Knott et al. [37] also predicted an interfacial free energy value of the CH_4 hydrate $\gamma_{hw} \approx 31\,mJ/m^2$ using similar technique.

More recently, some of us have investigated the nucleation of CH_4 hydrate using molecular dynamics simulations combining the Seeding technique [37,53,55] and CNT [77–79]. From these simulations, an interfacial free energy of approximately $38\,mJ/m^2$ was determined at 400 bar and 260 K, corresponding to a supercooling of about 35 K below the three-phase equilibrium temperature [49,50]. We have also employed the same techniques and molecular model for water to estimate the nucleation rate of CO_2 hydrate under the same pressure and supercooling conditions [74,80]. Our results indicate that the corresponding interfacial free energy is approximately $22\,mJ/m^2$. Although these values correspond to the interfacial free energy of both hydrates at supercooling conditions (35 K), they represent a difference of $16\,mJ/m^2$ of interfacial energy between both hydrate-water interfaces.

The estimation of interfacial free energies is intrinsically connected to the quantification of hydrate nucleation rates. Arjun and Bolhuis have examined the homogeneous nucleation of CO_2 and CH_4 hydrates using rigorous molecular simulation techniques, including Transition Path Sampling and Transition Interface Sampling [44,46,47,72,73]. The key finding is that the nucleation barrier for CO_2 hydrate is lower by several tens of k_BT compared to that of CH_4 hydrate under similar conditions [47]. In line with this, our recent findings exhibit the same trend [49–51,74] which we ascribe to differences in the interfacial free energies between the two hydrate systems.

A fundamental question remains: Are the interfacial free energies of CO_2 hydrate–water and CH_4 hydrate–water indeed different, as suggested by indirect methods, or are they comparable? Notably, all aforementioned estimates rely on indirect approaches. A more definitive answer could be obtained by employing a direct method to compute the interfacial free energies of both hydrates, thereby clarifying whether γ_{hw} differs between these systems.

The direct methods [63,75,81–93] allow for evaluation directly, without any theoretical approach, solid-fluid interfacial free energies in a straightforward manner. In general, the mechanical approach cannot be straightforwardly applied to solid–fluid interfaces, as it is difficult to account for the elastic response of deformable solids in a simple manner [75]. There are, however, important exceptions to the considerations outlined above that merit discussion. In cases where the solid phase is rigid, mechanical approaches become applicable. These methods are comparatively simpler and have been successfully employed to calculate both solid–liquid and solid–gas surface tensions [94].

The Mold Integration (MI) technique is the only direct method successfully used to predict with confidence the interfacial free energy of hydrate-water interfaces, including those of CO_2 and THF [75,80,95–97]. Fig. 1 shows schematically the basis of this methodology, which, starting from a definition of the water molecules belonging to the hydrate phase, allows one to induce the formation of a hydrate-water interface, and to reversibly estimate the work to form the interface and the interfacial free energy from thermodynamic integration.

The MI method employs a mold of attractive interaction sites that trap water molecules at specific crystallographic positions (cyan spheres in the snapshots shown in the center of Fig. 1). Each interaction site is characterized by a range, r_w, which governs the ability of the mold to suppress crystallization, induce nucleation, or overinduce full crystallization. In the original formulation of the method [98], an optimal value r_w^0 is defined such that the free energies of the hydrate and aqueous phases are equal, corresponding to coexistence conditions. The interfacial free energy, γ_{hw}, is then obtained in the limit $r_w \to r_w^0$.

Depending on the value of r_w, the mold may induce the formation of a thin hydrate layer, creating two planar hydrate–water interfaces (see snapshots at various stages of crystallization in Fig. 1). To characterize these processes, we employed optimized order parameters derived from the classical local-bond order metrics of Lechner and Dellago [99], which allow us to distinguish water molecules in liquid- or hydrate-like environments and to determine the size of the largest hydrate cluster, n_h. The temporal evolution of n_h, monitored across independent trajectories (shown in different colors in the right-hand panels of Fig. 1), reveals distinct crystallization scenarios as a function of the relative value of r_w with respect to r_w^0. For $r_w < r_w^0$, crystallization proceeds rapidly, as evidenced by the steep increase of n_h and the subsequent formation of the hydrate phase. When $r_w > r_w^0$, the system typically exhibits an induction period before crystallization eventually occurs (see yellow, blue, and green trajectories in the middle panel). The coexistence point r_w^0 lies between these regimes. Finally, for $r_w \gg r_w^0$, no complete hydrate layer forms; n_h remains essentially constant throughout the simulation, indicating that the system does not crystallize, although residual hydrate-like order persists ($n_h \neq 0$; see bottom panel of Fig. 1). Under these conditions, thermodynamic integration can be applied to compute the free-energy difference between the aqueous and hydrate phases. Extrapolating γ_{hw} to the limit $r_w \to r_w^0$ then yields the interfacial free energy at coexistence, as shown in the top-right panel of Fig. 1.

In this work, we apply two extensions of the MI method [80,95] to obtain independent estimates of the CH_4 hydrate–water interfacial free energy. This approach enables us to calculate γ_{hw} directly from its thermodynamic definition, without relying on theoretical models or additional computations. We present, for the first time, a direct calculation of the interfacial free energy for the CH_4 hydrate–water system using this approach. The resulting values are compared with those from our earlier studies based on robust indirect methodologies [50,74].

2. Simulation methods

2.1. Methodology

The MI technique is based on the use of a mold formed from N_w attractive interaction sites located at the crystallographic positions of one or several planes of the solid phase involved in the calculation of the interfacial free energy [98,100,101]. It is important to emphasize that different solid surfaces exposed to the liquid will generally yield different values of the interfacial free energy. For instance, in one of the original studies by Espinosa et al. [101], the interfacial free energy of Ih ice–liquid water, γ_{iw}, was determined using molds specifically designed for the various Ih ice surfaces. As expected, distinct values of γ_{iw} were obtained. This behavior arises from the hexagonal crystallographic structure of Ih ice, which presents three principal planes: basal, primary prismatic (pI), and secondary prismatic (pII). In contrast, the situation for CH_4 and CO_2 hydrates differs, as both adopt the cubic sI crystallographic structure. In this case, the principal planes of the cubic crystal belong to the same family of planes, {1,0,0}. Consequently, the interfacial free energy, γ_{hw}, is independent of the specific principal plane of the hydrate that is exposed to the liquid water phase. Naturally, if a different crystallographic plane were exposed to the liquid phase (for instance, by cleaving the hydrate along a distinct surface), the corresponding interfacial free energy would differ.

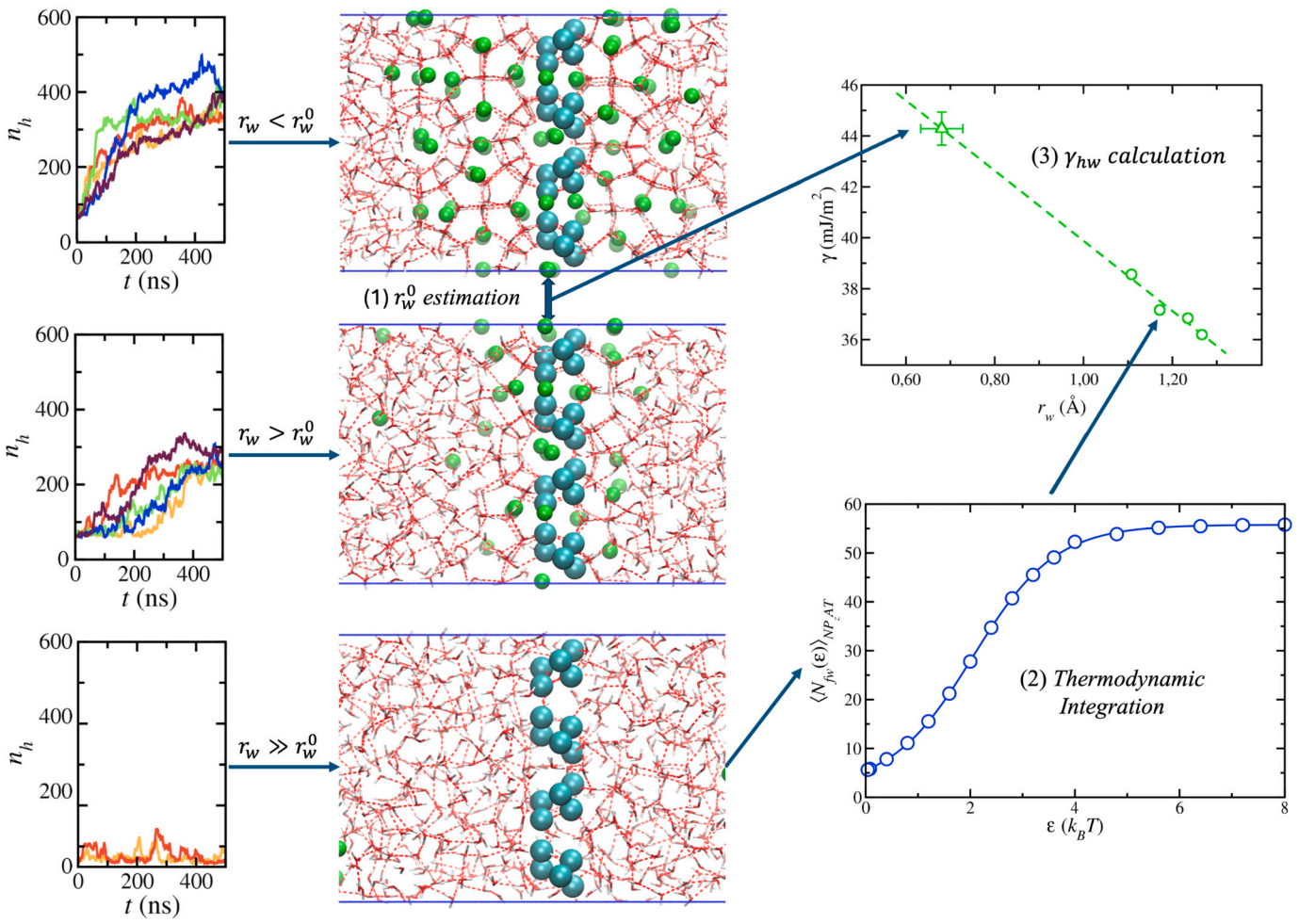

Fig. 1. Schematic representation of the MI-H technique. A collection of attractive sites (cyan spheres) is placed at the crystallographic positions of the oxygen atoms in the hydrate lattice to induce the formation of hydrate–water interfaces (middle). The growth of the hydrate phase is tracked by monitoring the number of water molecules (left) identified as solid-like (n_h). As a function of the water-attractive interaction sites range (r_w), three possible scenarios arise (Step 1, r_w^0 estimation), which allow us to identify the optimal interaction range (r_w^0) where the interfacial energy is determined. In Scenario I, $r_w < r_w^0$, the mold provides an excess of energy, and the system crystallizes as soon as the simulation begins. In Scenario II, $r_w > r_w^0$, the mold provides less energy than the interfacial free energy. It means that, in order to crystallize, the system must overcome a small free energy barrier, which is translated into an induction period during which crystallization does not occur until the energy barrier is overcome. Finally, Scenario III arises when $r_w >> r_w^0$ and the crystallization never takes place. Scenario III is where the thermodynamic integration (Step 2, Thermodynamic Integration) is carried out, since a phase transition will never occur, and Eq. (1) can be safely applied. Finally, by performing the thermodynamic integration at different r_w values, it is possible to extrapolate and calculate the interfacial free energy value at r_w^0 (Step 3, γ_{hw} calculation). Notice that in the case of the MI-G technique, the attractive sites were placed in the center of the hydrate cages.

The interaction between the molecules of the fluid system and the attractive interaction sites is based on a continuous version of the square-well potential [102]. These attractive interaction sites, which induce interactions between the mold and water molecules, are defined by two molecular parameters: the interaction range, r_w, and the well depth, ϵ. Further details on the implementation of this continuous square-well intermolecular potential for pure substances and hydrates can be found in the works of Espinosa et al. [98,101] and in our previous studies [80,95–97], respectively.

When the mold is switched off, water molecules diffuse freely in the fluid. As the mold is progressively switched on (by increasing the well depth, ϵ, from 0 to a maximum value ϵ_m), an increasing number of mold sites become occupied by water molecules. If r_w, the attractive interaction range of the wells, is sufficiently narrow, a CH_4 hydrate crystal slab forms around the mold sites. This parameter must therefore be small enough to ensure that each well accommodates only one water molecule once the mold is activated.

According to the Mold Integration methodology, the interfacial free energy depends on the specific choice of r_w used in the calculations. It is thus necessary to determine a priori the value that yields the correct estimate of γ_{hw}. This value is referred to as the optimal well radius, r_w^0. If $r_w < r_w^0$, the free energy of the hydrate phase becomes lower than that of the aqueous CH_4 solution, and the system rapidly transforms into the solid phase via a first-order phase transition—that is, the system freezes completely. This outcome is undesirable, since the method relies on computing the reversible work required to form a thin hydrate slab. As γ_{hw} is evaluated through thermodynamic integration while progressively switching on the mold, only reversible paths are valid. Therefore, Mold Integration must be applied exclusively for $r_w > r_w^0$.

As shown by Espinosa et al. [98], it is not advisable to perform thermodynamic integration at $r_w = r_w^0$, where the free energies of the hydrate and aqueous phases are equal. Instead, several calculations of γ_{hw} are performed for different values of r_w with $r_w > r_w^0$. The correct interfacial free energy at coexistence, γ_{hw}, is then obtained by extrapolating the function $\gamma_{hw}(r_w)$ to r_w^0.

In hydrates, it is possible to use two different types of molds of attractive interaction sites: one located at the crystallographic positions of the oxygen atoms of the molecules of water in the hydrate (MI-H) [80]

and other at the centers of the voids of each cage left by the hydrate structure (MI-G) [95]. See a representation of the initial configurations of the simulation boxes in Fig. S5 of the SI.

It is important to recall that the attractive interaction sites of the mold are switched on gradually to induce the formation of a solid hydrate slab in the fluid *at coexistence conditions*. The energy needed to form a thin crystal slab of the solid phase in the fluid phase can be computed by integrating the average number of filled attractive interaction sites (wells), $N_{fw}(\varepsilon)$, along a reversible thermodynamic path that links the fluid system without the solid hydrate slab (wells off), and the fluid system with the induced hydrate slab (wells completely on) [80,95,98]:

$$\Delta G^{hw} = N_w \epsilon_m - \int_0^{\epsilon_m} \left\langle N_{fw}(\varepsilon) \right\rangle_{NP_zAT} d\varepsilon \tag{1}$$

where ε and ϵ_m are the well depth and the maximum well depth, respectively, of the square-well potential. The average number of filled wells is obtained in the isothermal-isobaric ensemble to ensure that the system is always at the selected coexistence conditions of T and P. $\mathcal{A}$ represents the interfacial area between the hydrate and the aqueous solution of CH_4. Knowledge of ΔG^{hw} allows to determine the solid-fluid interfacial free energy γ_{hw} in a simple way,

$$\gamma_{hw} = \frac{\Delta G^{hw}}{2\mathcal{A}} \tag{2}$$

Factor 2 arises because two hydrate-fluid interfaces appear when the solid hydrate slab is induced. We refer the lector to our previous works [80,95,96] and Section 2.3 for further details.

2.2. Model

Water molecules are modeled using the well-known TIP4P/Ice [103] and CH_4 molecules are modeled using a spherical Lennard-Jones (LJ) interaction site with the parameters proposed by Guillot and Guissani [104] and Paschek [105]. Note that although CH_4 is a nonspherical molecule [106], this simple model has been used previously in the literature to determine the dissociation line of CH_4 hydrate in pure water [107–110] and in salty water at oceanic conditions [111], the solubility of CH_4 in water [49], and homogeneous nucleation rate of CH_4 hydrate formation [50]. It should be emphasized that, although highly simplified, it has been shown to deliver excellent quantitative results over a broad range of thermodynamic conditions [107–112]. Therefore, no significant impact on our results is expected from the use of this model. Nevertheless, it is worth noting that other authors, such as Fernández-Fernández and collaborators [113,114], have also employed more detailed all-atom models for CH_4, including TraPPE [115] and OPLS-UA [106].

The unlike interactions between water and CH_4 molecules are taken into account using the well-known Lorentz-Berthelot combining rules. The use of these rules ensures a good description of the dissociation line of the CH_4 hydrate, as well as other properties [49,50,107,108,110]. Particularly, this election provides a good estimation of the dissociation temperature of the methane hydrate at 400 bar using the direct coexistence technique, $T_3 = 294(2)$ K, and the solubility methodology, $T_3 = 295(2)$ K, recently used by Grabowska et al. [49]. This result is in excellent agreement with the experimental value, 297 K [1]. Note that a good estimate of the dissociation line of the hydrate is necessary to use with confidence the MI approach [80,95,96,98,101].

2.3. Simulation details

We use the GROMACS simulation package (version 4.6 in double precision) [116] to perform MD simulations via the isothermal-isobaric or NP_zAT ensemble [117–121] at 400 bar and 294 K using the MI-H [80] and MI-G [95] techniques. We place 736 water molecules surrounded by two pure liquid CH_4 phases with 128 molecules in each one in the initial simulation box. It should be noted that, in principle, finite-size effects may influence the interfacial free energy estimated using the Mold Integration technique. Indeed, in previous studies we have examined finite-size effects on the determination of hydrate dissociation lines, including those of CO_2 and CH_4 [110,112,122]. These analyses indicate that larger systems can display different dissociation temperatures (i.e., coexistence conditions) and, consequently, slightly different interfacial free energies. A comprehensive evaluation of these effects, however, lies beyond the scope of the present study and will be addressed in future work.

We arbitrarily choose the z-axis as perpendicular to the planar interfaces and the xy-plane parallel to the interfaces. The dimensions of the simulation boxes along the x and y-axis parallel to the water–methane planar interface are chosen to be consistent with the size of the CH_4 hydrate unit cell formed when the mold is switched on. The simulation box is a parallelepiped of volume $V = L_x \times L_y \times L_z$, where L_x, L_y, and L_z are the dimensions of the simulation box. L_x and L_y are kept constant, and only L_z is varied along the simulation to keep the pressure constant along the direction perpendicular to the planar interfaces. We first simulate a bulk CH_4 hydrate phase using the anisotropic version of the NPT ensemble at the equilibrium conditions under study. From this simulation is possible to determine the equilibrium dimensions of the simulation box (L_x, L_y, and L_z).

It is worth emphasizing that the rigorous framework for simulating phase coexistence across planar interfaces–namely, between the two liquid phases (aqueous CH_4 solution and pure liquid CH_4 in this work) as well as between the solid and fluid phases when the mold is activated to induce hydrate formation–is the isothermal-isobaric NP_zAT ensemble. This ensemble guarantees that the system is maintained at the correct equilibrium normal pressure, i.e., along the direction perpendicular to the hydrate slab formed upon mold activation [118–120]. This is accomplished by performing an independent simulation of the bulk solid phase at coexistence conditions (294 K and 400 bar) using the standard NPT ensemble, in which the three box lengths fluctuate independently [119]. Because CH_4 hydrate crystallizes in a cubic lattice, such a calculation could, in principle, also be carried out with the isotropic NPT ensemble [118,120]. Nevertheless, we chose to employ the fully anisotropic NPT ensemble in order to determine the equilibrium lattice constants along all three Cartesian directions. The motivation is that the solid-phase simulations were specifically designed to obtain the equilibrium values of L_x, L_y, and L_z under coexistence conditions (294 K and 400 bar), at which the interfacial free energy is evaluated. This procedure yields the equilibrium positions of the oxygen atoms in the water molecules of the hydrate phase–essential information for a reliable implementation of the Mold Integration technique. The equilibrium values obtained at 294 K and 400 bar, consistent with the hydrate unit cell under coexistence conditions, were subsequently employed in the NP_zAT simulations [80,95–98,100]. This ensures that the slab of hydrate induced by the mold, at the equilibrium conditions of pressure and temperature, is non-stressed [118–120].

Newton's equations are solved using the Verlet leapfrog algorithm [123]. We use a time step of 2 fs. All simulations are run in the NP_zAT ensemble to ensure that the pressure and the temperature are kept constant. The Nosé-Hoover thermostat [124] and the Parrinello-Rahman barostat [125] are used to keep both the temperature and the pressure constants. Simulations of the bulk solid phase to determine the equilibrium dimensions of the simulation box are run using the anisotropic version of the Parrinello-Rahman barostat. In all cases, we use 2 and 1 ps for the relaxation times in the thermostat and barostat, respectively. We use a cutoff radius for both dispersive and electrostatic interactions of 1 nm. Long-range interactions due to electrostatic interactions are determined using the Particle-Mesh Ewald technique [126]. We do not use long-range corrections for the dispersive

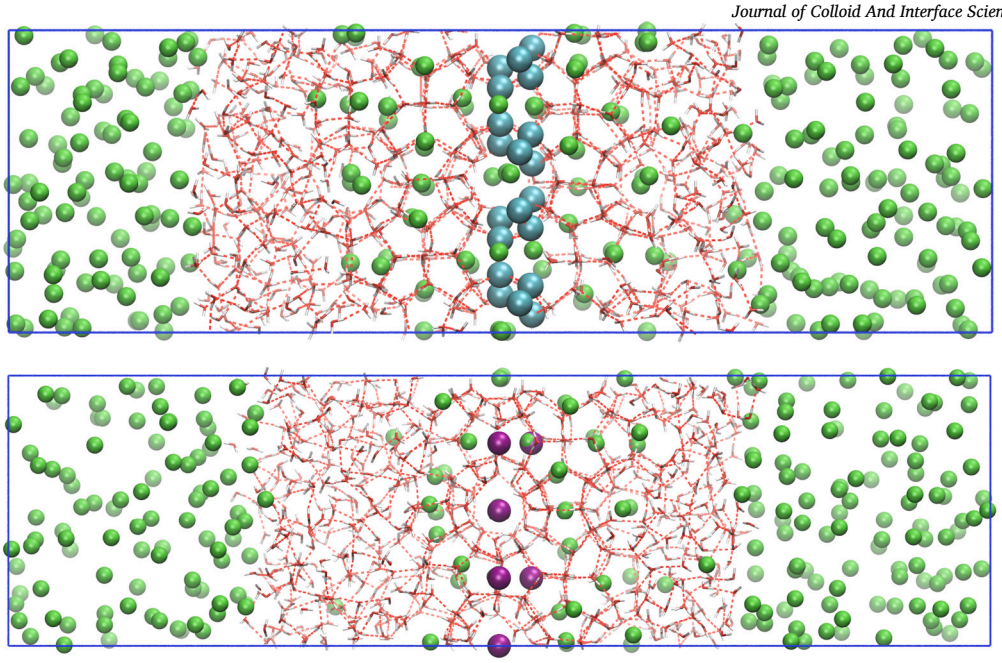

Fig. 2. Representation of the final configurations of simulation boxes using the MI-H (top) and the MI-G (bottom) approaches when $r_w < r_w^0$ at 400 bar and 294 K. In both cases, CH_4 molecules and water molecules are represented as green spheres and red and white sticks, respectively. Cyan and purple spheres represent the attractive interaction sites used in the MI-H and MI-G methods, respectively.

interactions. The LINCS algorithm is used in order to fix the molecular geometry.

For the calculation of the interfacial free energy we use $N_w = 56$ attractive sites with $\varepsilon_m = 8\,k_BT$ (MI-H) [80] and $N_w = 16$ attractive sites with $\varepsilon_m = 12\,k_BT$ (MI-G) [95]. We have chosen the same geometries used in our previous works to estimate the interfacial free energy of the CO_2 hydrate-water interface [80,95,96]. The attractive sites of both molds are used to induce the formation of a CH_4 hydrate slab in the middle of the simulation box. Fig. S3 of SI shows two snapshots of the initial simulation box with the mold used in this work.

3. Results and discussion

The MI methodology allows to determine the interfacial free energy in three steps [80,95,96,98,101]: (1) estimation of the optimal radius r_w^0; (2) calculation of the reversible work needed to form a thin crystal slab of the solid phase in the fluid phase and γ_{hw} at least three radii higher than the optimal one; and (3) extrapolation of γ_{hw} at r_w^0. This procedure is explained in the following sections.

3.1. r_w^0 estimation

The accurate determination of r_w^0 requires multiple simulations. By analyzing the behavior of the system for a series of different values of r_w, it is possible to find three different scenarios as a function of the r_w value. If $r_w < r_w^0$, the fluid phase becomes unstable and the fluid system crystallizes as soon as the simulation starts (scenario I) [80,95,96]. Fig. 2 presents the final configurations obtained from simulations employing both MI approaches, highlighting crystallization induced by molds activated with $r_w < r_w^0$. Representative snapshots from different stages of the simulations are shown in Figs. S1 and S2 of the Supporting Information (SI). Additionally, movies S1 and S2 illustrate the crystallization process observed with two extensions of the Mold Integration technique, the Mold Integration-Host (MI-H) and Mold Integration-Guest (MI-G) methods, under conditions where $r_w < r_w^0$. See Section 2.1 for further details. If $r_w > r_w^0$, and the value of r_w is closed to the optimal value, r_w^0, the system can overcome the energy barrier and crystallize after a relatively short period of time called induction period (scenario II). The larger the r_w value, the larger the time required by the system to crystallize. If r_w is large enough, the system will not crystallize because the energy barrier that the system has to overcome is too large (scenario III). Movies S3 and S4 of SI demonstrate that crystallization does not occur with either method when $r_w \gg r_w^0$. The optimal r_w^0 value is found in the frontier between scenarios I and II. Five independent trajectories have been run for each r_w in both methods at each r_w analyzed. Simulations have run for 500 ns to identify the behavior of the system, at each r_w, with one of the three possible scenarios explained previously.

To study the behavior of the system as a function of the r_w value, it is necessary to identify the number of molecules of water that transit from the aqueous fluid phase to the crystal hydrate phase. The number of molecules of water in the hydrate phase, as a function of the simulation time, $n_h = n_h(t)$, is analyzed using the local bond order parameters proposed by Lechner and Dellago [99] once the simulation has finished. In particular, the $\overline{q}_3$ parameter has been chosen to distinguish between liquid-like and CH_4 hydrate-like water molecules. This parameter has been previously used by some of us in our previous works about the CO_2 hydrate-water interfacial free energy [80,95,96]. For further technical details, we recommend our previous works [80,95,96] and our recent results extending this technique to deal with other hydrate structures [97,127].

We first consider the election of the optimal r_w^0 value using the MI-H technique (see Section 2.1). As can be seen in Fig. S3 of the SI, it is possible to identify the three mentioned scenarios as a function of r_w from the analysis of n_h. When $r_w \leq 0.823$ Å, the system crystallizes as soon as the simulations start, and consequently, these values correspond to Scenario-I. When $r_w \geq 0.855$ Å, large induction periods can be observed in at least one of the runs, and the behavior of the system can be categorized as the expected one in scenario II ($r_w > r_w^0$). Finally, when $r_w \geq 0.887$ Å, the system can not overcome the energy barrier, and no crystallization is observed as it is expected when $r_w \gg r_w^0$. This is the expected behavior found in scenario III.

In summary, r_w^0 is bounded between $r_w = 0.823$, Å (the largest value in scenario-I, corresponding to no induction behavior) and $r_w = 0.855$ Å (the smallest value in scenario-II, corresponding to induction behavior), as shown in Fig. S3 of the SI. Adopting a conservative estimate, we take

the lower and upper bounds as $r_w^{(l)} = 0.792$ Å and $r_w^{(u)} = 0.887$ Å. This yields a mean value $r_w^0 = (r_w^{(l)} + r_w^{(u)})/2 \approx 0.839$ Å and an uncertainty $\sigma_{r_w^0} = (r_w^{(u)} - r_w^{(l)})/2 \approx 0.048$ Å. The resulting optimal value is therefore $r_w^0 = 0.839(48)$ Å.

From this analysis, it is clear that the choice of $r_w = 0.839$ Å as the optimal value, r_w^0, since the change from scenario I and II is observed at exactly this value of r_w. Since free-energy calculations are extremely complex, in order to ensure that r_w^0 and, hence, γ_{hw}, are calculated with the appropriate uncertainty, a conservative range for r_w^0 has been chosen. In this case, the optimal value and its uncertainty is $r_w^0 = 0.839(95)$ Å.

For the MI-G calculations (see Section 2.1), r_w^0 is located between $r_w = 0.665$ Å (largest value in scenario-I) and $r_w = 0.697$ Å (smallest value in scenario-II), as shown in Fig. S4 of the SI. Following the same conservative procedure, we set $r_w^{(l)} = 0.633$ Å and $r_w^{(u)} = 0.728$ Å, giving $r_w^0 = (r_w^{(l)} + r_w^{(u)})/2 \approx 0.681$ Å with an uncertainty $\sigma_{r_w^0} = (r_w^{(u)} - r_w^{(l)})/2 \approx 0.048$ Å. The corresponding optimal value is $r_w^0 = 0.681(48)$ Å.

3.2. Thermodynamic integration

Interfacial energy can not be evaluated directly at $r_w = r_w^0$ because there is no energy barrier between the aqueous and the hydrate phase, i.e., the system can freely crystallize, crossing a first-order transition and moving away from the coexistence equilibrium. In order to create a thermodynamic path between the fluid without a solid hydrate slab (mold off) and the fluid with the solid hydrate slab (mold on), it is necessary to ensure that a phase transition does not occur. As Espinosa et al. [98] pointed out in their original work, it is necessary to perform the thermodynamic integration for $r_w > r_w^0$. This ensures the reversibility of the system, a necessary condition to calculate γ_{hw}.

In order to calculate ΔG^{hw}, we determine the average number of filled attractive sites, $\langle N_{fw} \rangle$, as function of the attractive interaction between the mold and the particles of the fluid system, ε. $\langle N_{fw} \rangle$ can be calculated by performing simulations in the isothermic-isobaric ensemble for different values of ε from 0 to ε_m ($\varepsilon_m = 8\,k_BT$ and $\varepsilon_m = 12\,k_BT$ for MI-H and MI-G techniques, respectively). Particularly, to accurately obtain $\langle N_{fw} \rangle$ as a function of ε, we perform between 17 and 21 simulations in the NP_zT ensemble depending if the MI-H or the MI-G technique is used. Each simulation is equilibrated during 20 ns and averages are calculated over 80 ns. Fig. 3 shows $\langle N_{fw} \rangle$, as functions of ε, as obtained from simulation results for the r_w values using both methodologies. We have also included the fitted curves in all the cases. As can be seen, when the mold is completely activated, the $\langle N_{fw} \rangle$ value at each r_w is equal to the total number of attractive sites located in the mold, N_w [98].

The difference in energy between the fluid state in which the mold is off ($\varepsilon = 0$) and the state in which the attractive sites of the mold are completely activated ($\varepsilon = \varepsilon_m$) has two contributions: one because of the creation of the hydrate-fluid interfaces and other due to the interaction between the mold and the molecules (water or methane depending on the MI technique used) in the system. The first contribution can be easily obtained from the integration of the fitted curves shown in Fig. 3 from $\varepsilon = 0$ to $\varepsilon = \varepsilon_m$, according to equations presented in Section 4. The second one, which accounts for the mold-molecule interaction energy ($-N_w\,\varepsilon_m$) of the final state (mold completely activated or $\varepsilon = \varepsilon_m$), can be easily subtracted from the thermodynamic integration contribution. Finally, once ΔG^{hw} has been calculated, the value of γ_{hw} for each r_w value can be easily obtained according to Eq. (2).

3.3. γ_{hw} calculation

As it has been explained in previous sections, when $r_w > r_w^0$, there exists yet an energy barrier that the system has to overcome in order to crystallize. It is necessary to obtain the value of γ_{hw} when $r_w = r_w^0$. Fig. 4 shows the interfacial free energy, as a function of r_w, obtained

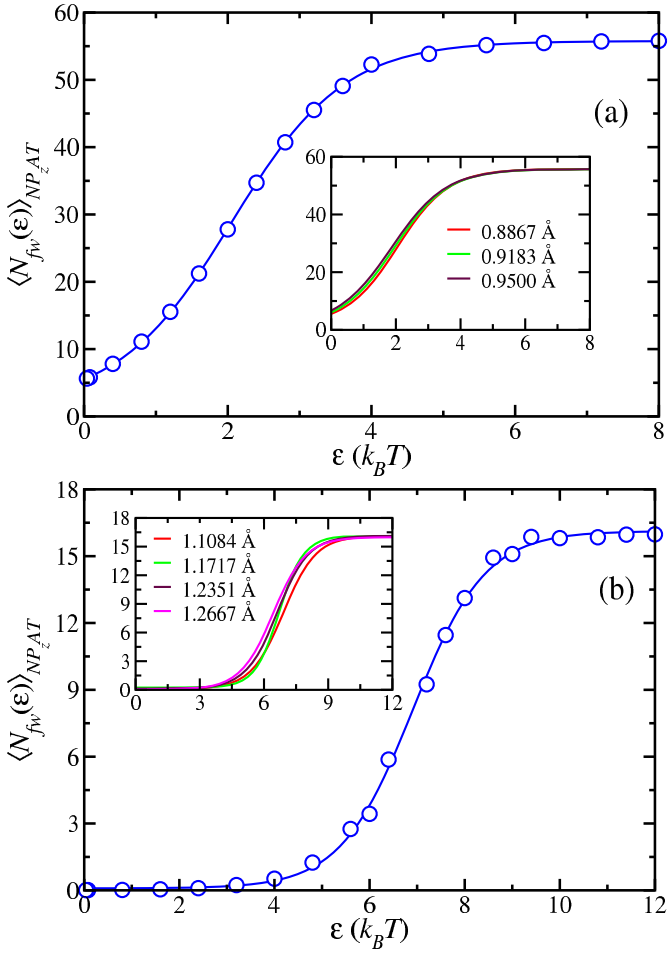

Fig. 3. Averaged number of filled attractive sites, $\langle N_{fw}(\varepsilon)\rangle_{NP_zAT}$, as a function of the well depth ε, obtained from MI-H at $r_w = 0.8867$ Å (top) and MI-G at $r_w = 1.1084$ Å (bottom) at 400 bar and 294 K. In both cases, in the main figure, the symbols represent the values of $\langle N_{fw}(\varepsilon)\rangle_{NP_zAT}$ from the NP_zT simulations, and the curves are obtained by fitting the simulation results. The insets represent the rest of the curves obtained for each r_w value used in both MI-H and MI-G methods. The value of r_w at which each curve has been obtained is shown in the legend.

from MI-H and MI-G techniques. As can be seen, γ_{hw} behaves linearly with the range of the attractive sites of the mold. Particularly, it is possible to calculate the real value of γ_{hw} by extrapolating the results as $r_w \to r_w^0$. It is important to mention that this behavior has been previously observed with different systems [56,80,95–98,100,101,128]. In all cases, MI provides interfacial free energies in excellent agreement with the experimental data.

According to the results presented in Fig. 4, the values obtained in the limit $r_w \to r_w^0$ are 42.57 and 44.28 mJ/m^2 for the MI-H and MI-G techniques, respectively. As in our previous work [80,95–97], we consider the main source of error in γ_{hw} to arise from the uncertainty in r_w^0. By construction, γ_{hw} lies at the midpoint of the interval $[\gamma_{hw}^{(l)}, \gamma_{hw}^{(u)}]$, where $\gamma_{hw}^{(l)}$ and $\gamma_{hw}^{(u)}$ are the values at $r_w = r_w^{(l)}$ and $r_w = r_w^{(u)}$. Specifically, $\gamma_{hw}^{(l)} = 44.43$ and $\gamma_{hw}^{(u)} = 40.67$ mJ/m^2 in the MI-H case, and $\gamma_{hw}^{(l)} = 44.93$ and $\gamma_{hw}^{(u)} = 43.64$ mJ/m^2 in the MI-G case. The uncertainties are then $\sigma_{\gamma_{hw}} = (\gamma_{hw}^{(u)} - \gamma_{hw}^{(l)})/2$, giving $\sigma_{\gamma_{hw}} \approx 1.88$ mJ/m^2 (MI-H) and 0.65 mJ/m^2 (MI-G). Thus, after rounding to the appropriate significant figures, the final interfacial free energy values with uncertainties are $\gamma_{hw} = 43(2)$ and 44(1) mJ/m^2 obtained from the MI-H and MI-G methodologies, respectively. As can be observed, the results obtained using the two techniques are in excellent agreement with each other. It is essential to emphasize

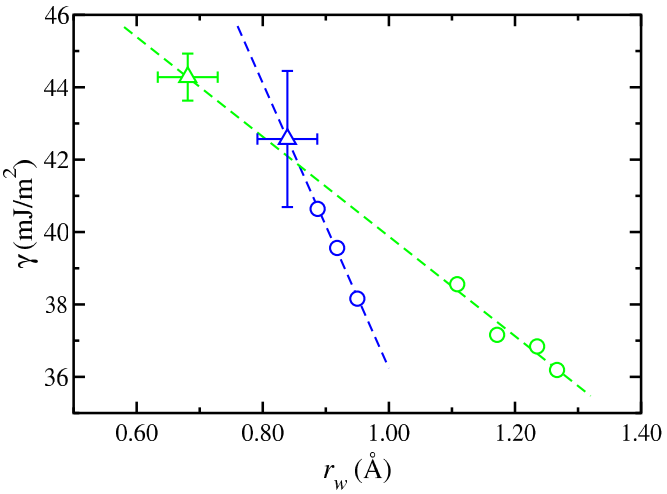

Fig. 4. CH_4 hydrate-water γ_{hw} as a function of r_w obtained from MI-H and MI-G methods at 400 bar and 294 K. Results from the MI-H method are shown in blue and those from the MI-G method in green. Dashed lines represent the fit of γ_{hw} as a function of r_w. Circles are used for data obtained from thermodynamic integration, while upward triangles denote extrapolated values of γ_{hw} obtained when $r_w \to r_w^0$.

that the results presented should be regarded as independent, as the key parameters employed in each method – namely, N_w, r_w, and ε_m – differ, as discussed in detail in Section 2.3.

It is possible to compare the predicted CH_4 hydrate-water γ_{hw} values obtained from simulation with experimental data obtained by Uchida et al. [68,69], 39 and 34(6) mJ/m^2. Note that both values are the same within the statistical uncertainty, although there exists a difference of 5 mJ/m^2 between both results. Anderson et al. [70,71] have also independently determined γ_{hw} values using the same indirect technique and thermodynamic relationship: between 32(1) and 35(1) mJ/m^2, given a final vale of 32(3) mJ/m^2. In summary, all the CH_4 hydrate-water interfacial free energy values obtained from experiments range in the interval from 28 to 40 mJ/m^2. This is a huge range of values and contrasts with the accuracy of the measurements available in the literature for the interfacial tension of liquid water at ambient conditions, 72 mJ/m^2, showing that the experimental determination of solid-fluid interfacial energies is a difficult task [57–59].

Simulation data obtained in this work, 43(2) and 44(1) mJ/m^2, seem to overestimate the experimental value reported by Anderson and collaborators [70,71], but they are in good agreement with the value reported by Uchida and coworkers, 39 mJ/m^2 [68]. This is the first time the Mold Integration methodology, a direct computer simulation method used to predict interfacial free energies of a wide variety of different model and realist systems [75], seems not to fully reproduce the experimental hydrate-fluid interfacial energies. Is the CH_4 hydrate-water interfacial system the limit of applicability of the Mold Integration method? We think the answer is no and will try to justify why.

To answer this question, we first compare the simulation results obtained from the MI direct technique with values previously obtained in the literature using indirect computer simulation methods. Jacobson and Molinero [35], using the mW water model [129], estimated a value of $\gamma_{hw} \approx 36(2)$ mJ/m^2. Note that this value corresponds to the case of a hydrate in which the guest molecule has intermediate properties between CH_4 and CO_2. This value lies between the experimental value for the CO_2 hydrate-water interface [71], 32(3) mJ/m^2, and that for the CH_4 hydrate-water interfacial energy [68], 39 mJ/m^2. This suggests that γ_{hw} is closer to 40 than to 30 mJ/m^2. One year later, Knott et al. [37] obtained a value for the interfacial free energy, $\gamma_{hw} = 31$ mJ/m^2.

However, one must be careful with the predictions obtained using this water model to predict γ_{hw} values. Although the successful mW model can predict a great variety of properties and systems, the original version of the mW model is parameterized to match the experimental vaporization enthalpy, liquid water density, and hexagonal ice melting temperature [130]. It is important to recall in this context that the prediction of hydrate – water interfacial free energy values critically depends on an accurate determination of the hydrate – water – guest three-phase equilibrium temperature. However, this model is found to overestimate the melting temperature of methane hydrate by $\sim 15 - 20$ K [32,131,132]. Particularly, Jin and Zhong [132] have recently reparameterized the mW model to accurately predict the experimental phase diagram of methane hydrate. They have shown that the phase stability of methane hydrate depends on the spring constant λ of the mW model, which determines the strength of the tetrahedral angle formed by three water molecules in the mW model. It would be interesting in the future to determine the CH_4 hydrate – water interfacial free energy using the parametrization proposed by these authors.

It is clear that previous works in the literature suggest that the hydrate-water interfacial energy of the CH_4 and CO_2 hydrates are similar and also around the value of the ice-water interfacial energy, $\sim$ 30 mJ/m^2 [35,68–71]. However, our current results indicate that the CH_4 hydrate-water γ_{hw} value is substantially higher than that of the CO_2 hydrate – water interface, in agreement with estimations from their nucleation rates [50,74]. In the next section, we compare both results to clarify and understand from a microscopic perspective the reasons for which interfacial free energies of CH_4 and CO_2 hydrates seem to be different.

Before addressing this point, it is useful to propose an independent hypothesis regarding the underlying mechanism. Unfortunately, providing a detailed molecular explanation of why the interfacial free energy of CH_4 hydrate is higher than that of CO_2 hydrate is an extremely challenging task [74]. In fact, interfacial free energy is, by definition, a free energy quantity, and its evaluation from computer simulations—whether using molecular dynamics or Monte Carlo techniques—is inherently difficult because free energy is a non-mechanical property. It cannot be directly obtained as a simple ensemble average of a microscopic observable.

Can one, in principle, gain deeper insight into how guest–host coupling and the enthalpic and entropic contributions influence the interfacial energy of CH_4 and CO_2 hydrates? We believe so; however, as mentioned above, such an analysis would require a very demanding and specialized study, which lies beyond the scope of the present work. The main goal of this study is rather to obtain the first realistic and accurate estimation of the CH_4 hydrate–water interfacial free energy using a direct computer simulation approach.

Nevertheless, it is possible to propose a physically sound and qualitative explanation for why the interfacial free energy of CH_4 hydrate is higher than that of CO_2 hydrate, based on simple yet rigorous arguments. One of the most widely used families of empirical correlations for estimating vapor–liquid surface tension in real substances is the so-called Parachor approach, originally introduced by Macleod in 1923 [133]. In this method, the surface tension is correlated with the difference in bulk coexistence densities. Guggenheim later refined this correlation and estimated the corresponding exponent [134]. Although both approaches are empirical, their functional forms are supported by theoretical considerations rooted in the modern framework of renormalization group and scaling theories [135].

By analogy, extending these arguments to solid–fluid coexistence suggests that when the composition of the fluid phase becomes more similar to that of the hydrate phase [74], the interfacial free energy should decrease. The higher interfacial free energy, γ_{hw}, obtained for the CH_4 hydrate–water interface would therefore arise from the larger compositional difference between the aqueous phase and the hydrate. In contrast, the higher solubility of CO_2 in water reduces this compositional mismatch, leading to a significantly lower value of γ.

In fact, this hypothesis is further supported by independent results obtained for the THF hydrate–water interface. Using the MI technique, some of us calculated γ_{hw} [97] and compared it with experimental data

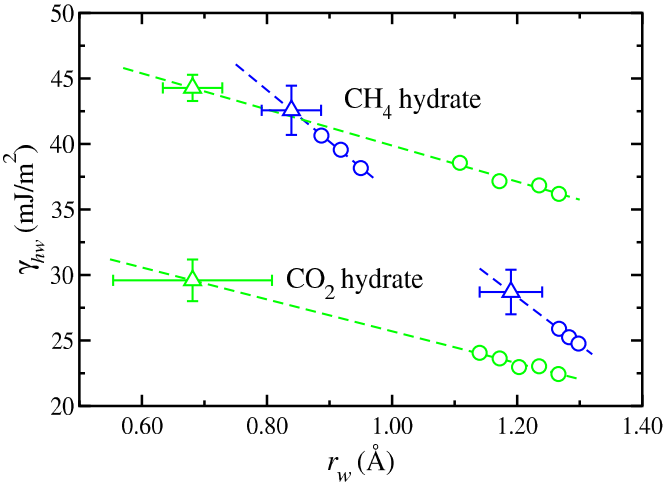

Fig. 5. CH_4 (top results) and CO_2 (bottom results) hydrate-water γ_{hw} as a function of r_w obtained from MI-H and MI-G methods at 400 bar, 294 K (CH_4), and 287 K (CO_2). Results from the MI-H method are shown in blue and those from the MI-G method in green. Dashed lines represent the fit of γ_{hw} as a function of r_w. Circles are used for data obtained from thermodynamic integration, while upward triangles denote extrapolated values of γ_{hw} obtained when $r_w \to r_w^0$. Results for the CO_2 hydrate are taken from out previous works [80,95,96].

available in the literature [136,137]. The experimental value of γ_{hw} is 24(8) mJ/m^2, while our MI calculations yield 27(2) mJ/m^2, showing very good agreement. In this case, γ_{hw} is much lower than the corresponding values for CH_4 and CO_2 hydrates. According to our hypothesis, this is an expected outcome, since THF is soluble in water under the conditions where the hydrate forms, and this solubility leads to a decrease in γ_{hw} compared with the CH_4 and CO_2 hydrate interfaces.

3.4. Comparison between γ_{hw} values of the CH_4 and CO_2 hydrates

We compare the results of γ_{hw} obtained in this work for the CH_4 hydrate with the results obtained by some of us [80,95,96] for the hydrate of CO_2. Fig. 5 shows the CH_4 hydrate- and CO_2 hydrate-water interfacial free energy values, as functions of r_w, obtained from MI-H and MI-G techniques. In both systems, the interfacial free energy between the hydrates and the aqueous phase has been obtained at 400 bar and coexistence conditions.

As can be seen, the γ_{hw} values obtained in this work for the CH_4 hydrate, 43(2) and 44(1) mJ/m^2, are about 40% higher than that for the CO_2 hydrate at practically the similar thermodynamic conditions (29(2), 30(2) and 31(2) mJ/m^2) [80,95,96]. Is this real? To check this hypothesis, we compare these results with estimations provided by the Seeding combined with CNT approach using the same molecular models and under the same conditions of temperature and pressure for CH_4 and CO_2 hydrates.

Although the reader can see the results in both publications, to clarify the main result, we summarize the most essential conclusions obtained by these authors. According to CNT, the homogenous nucleation rate can be expressed as [28,30,31,50,74,138],

$$J = \rho_G Z f^+ e^{-\Delta G_c/k_B T} = J_0\, e^{-\Delta G_c/k_B T} \tag{3}$$

where ρ_G is the guest (CO_2 or CH_4) density in the aqueous solution phase, Z the Zeldovich factor, f^+ the attachment rate or rate at which CO_2 and CH_4 molecules in the aqueous phase attach to a growing solid cluster, and ΔG_c the nucleation barrier. Following the thermodynamic formalisms of Gibbs [139], the Zeldovich factor Z and the nucleation barrier ΔG_c, can be easily expressed in terms of the driving force for nucleation, $\Delta\mu_N$, and the size of critical solid clusters in both hydrates, N_c,

Table 1
Parameters that control homogeneous nucleation rates of CH_4 and CO_2 hydrates in water: guest density in the aqueous solution, ρ_G, hydrate density, ρ_H, Zeldovich factor, Z, size of the critical solid cluster (in terms of guest molecules), N_c^G, attachment rate, f^+, nucleation barrier, ΔG_c, driving force for nucleation, $\Delta\mu_N$. We also include homogeneous nucleation rate, J, and hydrate – water interfacial free energy, γ. In all cases, parameters have been obtained at 400 bar and supercooling temperature of 35 K. All the values have been taken from the works of Grabowska et al. [50] and Zerón et al. [74].

Parameter	CO_2 hydrate	CH_4 hydrate
$\rho_G/(m^3)$	2.6×10^{27}	3.0×10^{26}
$\rho_H/(m^3)$	4.7×10^{27}	4.6×10^{27}
N_c^G	20	83
$\Delta\mu_N/k_BT$	−2.26	−2.42
Z	0.077	0.039
f^+/s	6.5×10^{8}	1.4×10^{9}
$\Delta G_c/k_BT$	22.6	100.7
$J/(m^3\,s)$	2×10^{25}	3×10^{-10}
γ_{hw} (mJ/m^2)	18.7	32.5

$$Z = \sqrt{\frac{|\Delta\mu_N|}{6\pi k_B T N_c}} \tag{4}$$

and

$$\Delta G_c = \frac{1}{2} N_c |\Delta\mu_N| \tag{5}$$

Vega and collaborators [49,50] and Blas and collaborators [51,74] have determined, at the same pressure, 400 bar, and supercooling temperature, 35 K, all the parameters included in Eqs. (3)–(5). Table 1 summarizes the parameters that determine homogeneous nucleation rates of both hydrates.

The kinetic prefactor of the nucleation rate in Eq. (3), $J_0 = \rho_G Z f^+$, can be easily obtained from data presented in Table 1. According to this, the J_0 value for both hydrates only exhibits a difference of one order of magnitude since $J_0 \sim 10^{35}$ and $\sim 10^{34}$ m^{-3} s^{-1} for the CH_4 and CO_2 hydrates, respectively. However, according to the results presented by Grabowska et al. [50] and Zerón et al. [74], the nucleation rates of the CH_4 and CO_2 hydrates, at the same pressure and supercooling temperature, are $J \sim 10^{-10}$ and $\sim 10^{25}$ m^{-3} s^{-1}, respectively. The difference between both nucleation rates is huge. In fact, the nucleation rate of CO_2 hydrate is approximately 35 orders of magnitude larger than that for CH_4 hydrate under the same conditions. What is the reason for this difference?

Following Grabowska et al. [50] and Zerón et al. [74], the difference must stem from the exponential free energy barrier, which consists of two components: $\Delta\mu_N$ and N_c according to Eq. (5). While the $\Delta\mu_N$ values differ and trend in the expected direction, the variation alone does not appear significant enough to account for the disparity in nucleation rates. Instead, the primary factor is N_c, which includes 83 CH_4 molecules but only 20 CO_2 molecules under the same conditions. This distinction is crucial: the critical cluster of CO_2 hydrate is significantly smaller than that of CH_4 hydrate. In terms of free energy barrier values, the differences are huge at the same thermodynamic conditions: the CH_4 hydrate nucleation barrier is $\Delta G_c^{CH_4} \sim 100\, k_BT$ and that of the CO_2 hydrate is $\Delta G_c^{CO_2} \sim 23\, k_BT$. This difference is obviously the reason for the difference in the J values of both hydrates. However, what is the physical origin of this difference? To investigate it, the authors took into account the relationship that describes the nucleation barrier in terms of $\Delta\mu_N$ and the hydrate-water interfacial free energy, γ_{hw}, [50,74],

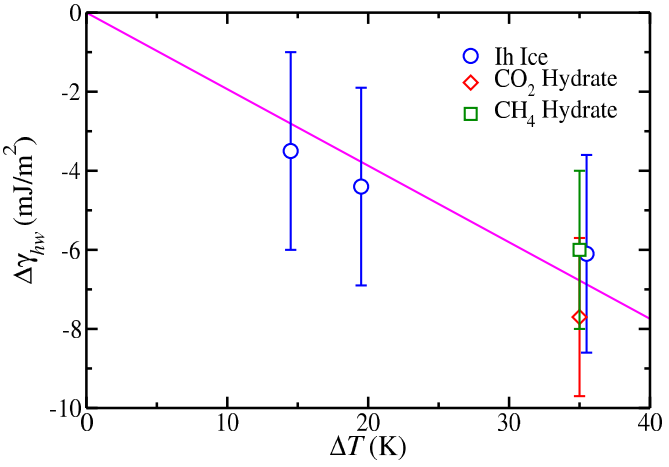

Fig. 6. Difference between the interfacial free energy at a given supercooling, ΔT, and the interfacial free energy at coexistence ($\Delta T = 0$ K), obtained for Ih ice – water (blue circles) [140], CO_2 hydrate – water (red triangle) [74], and CH_4 hydrate – water (green square) [50]. The magenta line represents the linear correlation of the data with ΔT given by Eq. (7).

$$\Delta G_c = \frac{16\pi\gamma_{hw}^3}{3\rho_H^2|\Delta\mu_N|} \tag{6}$$

As can be seen, the key to these differing behaviors lies in the interfacial free energy γ_{hw}, which is further amplified as it is raised to the third power. Note that ρ_H and $|\Delta\mu_N|$ values for both hydrate are similar. Particularly, the CO_2 and CH_4 hydrates – water interfacial free energy values obtained by Grabowska et al. [50] and Zerón et al. [74], using the Seeding technique and CNT are $\gamma_{hw}^{CO_2} = 18.7\,mJ/m^2$ and $\gamma_{hw}^{CH_4} = 32.5\,mJ/m^2$. In other words, there exists a difference between both interfacial energies is $\gamma_{hw}^{CH_4} - \gamma_{hw}^{CO_2} \sim 14\,mJ/m^2$.

It is interesting to compare this difference with that obtained using the interfacial free energy values of both hydrates obtained using the MI-H and MI-G techniques. According to our previous works [80,95,96], $\gamma_{hw}^{CO_2} = 29(2)$, 30(2), and 31(2) mJ/m^2. One can estimate the mean value for and uncertainty for this interfacial energy (taking into account all the values) as $\gamma_{hw}^{CO_2} = 30(3)\,mJ/m^2$. Similarly, the interfacial energy of the CH_4 hydrate – water interface obtained in this work is $\gamma_{hw}^{CH_4} = 43(2)\,mJ/m^2$. Note that this value and its uncertainty account for the two values previously presented. With this information, one can estimate the difference between both interfacial energies using these direct mehotds as $\gamma_{hw}^{CH_4} - \gamma_{hw}^{CO_2} \sim 13(4)\,mJ/m^2$. This is an interesting exercise. However, the values obtained from Seeding and CNT approaches correspond to interfacial energies of spherical hydrate clusters (and not planar hydrate – water interfaces) at supercooling conditions ($\Delta T = 35$ K). The γ_{hw} values obtained in this work correspond to planar hydrate – water interfaces at coexistence conditions (hydrate – water – guest), and it is not possible to compare directly both results. Fortunately, as we show in the following paragraphs, it is feasible to estimate $\gamma_{hw}^{CH_4}$ and $\gamma_{hw}^{CO_2}$ at the same conditions.

The first step is to get the interfacial free energy values of the planar interfaces. Montero de Hijes et al. [141] have demonstrated that the solid-fluid interfacial energy varies linearly with $1/R_c$, with R_c the radius of a critical solid cluster obtained from the Seeding technique. Specifically, they identified this relationship across multiple systems, including hard-sphere and Lennard-Jones simplified models, as well as more advanced force fields for water, such as mW and TIP4P/Ice for different supercoolings. In addition, Gabrowska et al. [50] and Zerón et al. [74] have also found the same behavior for the CH_4 and CO_2 hydrates. This insight has allowed all these authors to estimate, from Seeding calculations and CNT, the interfacial free energy of the corresponding planar solid-fluid interface (but not at coexistence conditions). They extrapolated γ_{hw} to the planar interface ($R_c \to \infty$) for different γ_{hw} values from different critical solid clusters.

Table 2
Estimated Interfacial energy γ_{hw}, as a function of the undercooling ΔT, for I_h ice – water, [140] CH_4 hydrate – water, [50] and CO_2 hydrate – water [74] with planar interface using Seeding-CNT techniques. Values at $\Delta T = 0$ are calculated by MI approach, [80,95,96,101] including those determined in this work. $\Delta\gamma_{hw} = \gamma_{hw}(\Delta T) - \gamma_{hw}(0)$ is the interfacial free energy at supercooling ΔT and at coexistence ($\Delta T = 0$ K).

ΔT(K)	γ_{hw}(mJ/m^2)	$\Delta\gamma_{hw}$(mJ/m^2)
I_h ice – water interface		
0	29.8(2.5)	0
14.5	26.3	-3.5(2.5)
19.5	25.4	-4.4(2.5)
35.5	23.7	-6.1(2.5)
CH_4 hydrate – water interface		
0	44(2)	0
35	38	-6(2)
CO_2 hydrate – water interface		
0	30(2)	0
35	22.3	-7.7(2)

Table 2 shows the values of interfacial energies (for planar interfaces) associated with the CH_4 hydrate – water [50] and CO_2 hydrate – water [74] interfaces at different supercoolings. For reasons that will be clear in the next paragraph, we have also included the values corresponding I_h ice – water interfacial free energies, at different supercooling values, as obtained from Seeding and CNT calculations by Espinosa et al. [140] See the original works of these authors for further details. Table 2 also included the I_h ice – water [101], CH_4 hydrate – water, and CO_2 hydrate water [80,95,96] interfacial energy values at coexistence conditions, $\Delta T = 0$ K, determined using the Mold Integration technique at coexistence conditions, 29.8(2.5), 43(2), and 30(2) mJ/m^2, respectively. Note that the value corresponding to the CH_4 hydrate – water interface, 43(2) mJ/m, has been obtained in this work.

We also define $\Delta\gamma_{hw}$ as the difference between $\gamma_{hw}(\Delta T)$, the interfacial free energy at a given supercooling, and $\gamma(0)$, the interfacial free energy at coexistence ($\Delta T = 0$ K), obtained from the MI technique for all the systems in Table 2. According to this, $\Delta\gamma_{hw} = \gamma_{hw}(\Delta T) - \gamma_{hw}(0)$, becomes more negative as ΔT increases. The results obtained previously for I_h ice – water by Espinosa et al. [101,140] and for CO_2 hydrates – water [74,80,95,96] follow this trend. Using this information, it is possible to represent $\Delta\gamma_{hw}$, as a function of ΔT, for the systems considered in Table 2. As can be seen in Fig. 6, $\Delta\gamma_{hw}$ shows a linear correlation with ΔT, represented by the continuous magenta line,

$$\Delta\gamma_{hw} = -0.194\,\Delta T\,(mJ/m^2) \tag{7}$$

It is worth noting that the linear regression was performed under the constraint that the line passes through the origin. This is fully justified since $\Delta\gamma_{hw}$ at $\Delta T = 0$ K must vanishes since $\gamma_{hw}(\Delta T) \to \gamma_{hw}(0)$ as $\Delta T \to 0$. The regression indicates that γ_{hw} decreases $\sim 0.19\,mJ/m^2$, approximately, for each K, the temperature is decreased with respect to the coexistence temperature. It is easy to check that if we apply it to the CO_2 hydrate – water interface obtained from CNT + Seeding calculations gives the value obtained from the direct MI technique, i.e., $\gamma(0) \equiv \gamma_{hw} = \gamma_{hw}(\Delta T) - \Delta\gamma_{hw} = 22.3 + 0.194 \times 35 \approx 29\,mJ/m^2$, which is in excellent agreement with the value obtained by Blas and collaborators using the MI-H and MI-G methodologies [80,95,96], 30(2) mJ/m. Using

the same approach, the estimation of the CH_4 hydrate – water interfacial free obtained from CNT + Seeding calculations of Zerón et al. [74] and Eq. (7), is $\gamma(0) \equiv \gamma_{hw} = \gamma_{hw}(\Delta T) - \Delta\gamma_{hw} = 38 + 0.194 \times 35 \approx 45\,\mathrm{mJ/m^2}$, which is also in excellent agreement with the value obtained in this work, $44(2)\,\mathrm{mJ/m^2}$.

4. Conclusion

In this work, we have determined the interfacial free energy between methane hydrate and liquid water using molecular dynamics simulations. To this end, we employed two recent extensions of the mold integration method, Mold Integration–Host (MI-H) and Mold Integration–Guess (MI-G), previously introduced by some of us [80,95] to address the challenges inherent to clathrate hydrate interfaces. All calculations were conducted under thermodynamic conditions in which the hydrate and aqueous phases coexist, as required by the methodology.

Recognizing the critical role of molecular models in determining interfacial free energies, we adopted the TIP4P/Ice water model, known for its accurate prediction of the ice–water interfacial energy [103], Methane was represented as a single-site Lennard-Jones particle, using parameters from Guillot and Guissani [104] and Paschek [105]. This combination of models has been shown to reliably reproduce the hydrate dissociation line [107,108], thus providing a robust framework for assessing interfacial properties at coexistence.

Using the MI-H and MI-G techniques, we obtained values of 43(1) and 44(1), $\mathrm{mJ/m^2}$, respectively, for the CH_4 hydrate–water interfacial free energy. These results, averaging around $44\,\mathrm{mJ/m^2}$, are notably higher than the values reported for CO_2 hydrate–water and ice–water interfaces ($\sim 30\,\mathrm{mJ/m^2}$). While the MI methodology has successfully reproduced experimental values for CO_2 hydrate [80,95,96] and ice [101], agreement with available experimental data for CH_4 hydrate remains less definitive. Experimental estimates span a broad range, from 28 to $40\,\mathrm{mJ/m^2}$ in the studies by Uchida et al. [68,69] and from 29 to $35\,\mathrm{mJ/m^2}$ in those by Anderson et al. [70].

Nonetheless, our results are consistent with previous simulation studies employing indirect approaches based on the same molecular models [74]. Furthermore, advanced computational studies of hydrate nucleation, both by Arjun and Bolhuis [44,46,47,72,73] and by some of us [74], have demonstrated that nucleation barriers for CH_4 hydrate are significantly higher than those for CO_2 hydrate under comparable conditions, by several tens of k_BT. Recent results from the Seeding technique combined with CNT also support this trend [74]. These differences in nucleation behavior have been attributed to underlying disparities in interfacial free energies, reinforcing our conclusion that the CH_4 hydrate–water interfacial free energy exceeds that of its CO_2 counterpart.

In summary, our results establish molecular simulation as a powerful and reliable complementary approach for determining interfacial free energies of hydrate systems. We demonstrate that the MI methodology enables accurate prediction of interfacial free energies for complex solid phases, including CO_2, THF, and CH_4 hydrates. This work represents a significant step forward in the molecular-level understanding of hydrate interfaces and opens new avenues for the computational determination of interfacial properties in a broad range of hydrate materials.

CRediT authorship contribution statement

Iván M. Zerón: Methodology, Investigation. **José Manuel Míguez:** Methodology, Investigation. **Jesús Algaba:** Writing – review & editing. **Bruno Mendiboure:** Investigation, Formal analysis. **Felipe J. Blas:** Writing – review & editing, Funding acquisition.

Declaration of competing interest

The authors declare that they have no known competing financial interests or personal relationships that could have appeared to influence the work reported in this paper.

Acknowledgement

Dedicated to Professor Pedro J. Pérez on the occasion of his 60th birthday. With gratitude for his valuable guidance as Director of the Center for Research in Sustainable Chemistry (CIQSO) and for the impetus he has inspired in us to pursue better and higher-quality science. We also thank Carlos Vega for helpful discussions. This work was financed by MCIN/AEI/10.13039/501100011033 (grant Refs. PID2021-125081NB-I00 and PID2024-158030NB-I00) and EU FEDER, and Universidad de Huelva (P.O. FEDER EPIT1282023), also cofinanced by EU FEDER funds. We also acknowledge Barcelona Supercomputing Center in Mare Nostrum under Grant No. FI-2023-2-0041 and Centro de Supercomputación de Galicia (CESGA, Santiago de Compostela, Spain) for providing access to computing facilities.

Appendix A. Supplementary material

Supplementary material related to this article can be found online at https://doi.org/10.1016/j.jcis.2025.139477.

Data availability

Data will be made available on request.

References

[1] E.D. Sloan, C. Koh, Clathrate Hydrates of Natural Gases, 3rd edition, CRC Press, New York, 2008.
[2] B.C. Barnes, A.K. Sum, Advances in molecular simulations of clathrate hydrates, Curr. Opin. Chem. Eng. 105 (2013) 184–190.
[3] J.A. Ripmeester, S. Alavi, Clathrate Hydrates: Molecular Science and Characterization, Wiley-VCH, Weinheim, Germany, 2022.
[4] J.-A. Dolyniuk, B. Owens-Baird, J. Wang, J.V. Zaikina, K. Kovnir, Clathrate thermoelectrics, Mater. Sci. Eng., R Rep. 108 (2016) 1–46.
[5] J.S. Kasper, P. Hagenmuller, M. Pouchard, C. Cros, Clathrate structure of silicon Na_8Si_{46} and Na_xSi_{136} ($x < 11$), Science 150 (1965) 1713–1714.
[6] H. Lin, S. Lee, L. Sun, M. Spellings, M. Engel, S.C. Glotzer, C.A. MirkinX, Clathrate colloidal crystals, Science 355 (2017) 931–935.
[7] S. Lee, E.G. Teich, M. Engel, S.C. Glotzer, Entropic colloidal crystallization pathways via fluid–fluid transitions and multidimensional prenucleation motifs, Proc. Natl. Acad. Sci. USA 116 (2019) 14843–14851.
[8] W.L. Mao, H.K. Mao, A.F. Goncharov, V.V. Struzhkin, Q. Guo, J. Hu, J. Shu, R.J. Hemley, M. Somayazulu, Y. Zhao, Hydrogen clusters in clathrate hydrate, Science 297 (2002) 2247–2249.
[9] E.D. Sloan, Fundamental principles and applications of natural gas hydrates, Science 426 (2003) 353–359.
[10] C.A. Koh, A.K. Sum, E.D. Sloan, State of the art: natural gas hydrates as a natural resource, J. Nat. Gas Sci. Eng. 8 (2012) 132–138.
[11] Z.R. Chong, S.H.B. Yang, P. Babu, P. Linga, X.-S. Li, Review of natural gas hydrates as an energy resource: prospects and challenges, Appl. Energy 162 (2016) 1633–1652.
[12] J. Zheng, Z.R. Chong, M.F. Qureshi, P. Linga, Carbon dioxide sequestration via gas hydrates: a potential pathway toward decarbonization, Energy Fuels 34 (2020) 10529–10546.
[13] C. Bourry, J.-L. Charlou, J.-P. Donval, M. Brunelli, C. Focsa, B. Chazallon, X-ray synchrotron diffraction study of natural gas hydrates from African margin, Geophys. Res. Lett. 34 (22) (2007).
[14] M. Yousuf, S. Qadri, D. Knies, K. Grabowski, R. Coffin, J. Pohlman, Novel results on structural investigations of natural minerals of clathrate hydrates, Appl. Phys. A 78 (2004) 925–939.
[15] Y.F. Makogon, Hydrates of Hydrocarbons, PennWell Publishing Co., Tulsa, OK, 1997.
[16] H. Aghajari, M.H. Moghaddam, M. Zallaghi, Study of effective parameters for enhancement of methane gas production from natural gas hydrate reservoirs, Green Energy Environ. 4 (2019) 453–469.
[17] A.Y. Manakov, S.V. Goryainov, A.V. Kurnosov, A.Y. Likhacheva, Y.A. Dyadin, E.G. Larionov, Clathrate nature of the high-pressure tetrahydrofuran hydrate phase and some new data on the phase diagram of the tetrahydrofuran-water system at pressures up to 3 GPa, J. Phys. Chem. B 107 (2003) 7861–7866.
[18] T. Makino, T. Sugahara, K. Ohgaki, Stability boundaries of tetrahydrofuran + water system, J. Chem. Eng. Data 50 (2005) 2058–2060.
[19] K.A. Kvenvolden, Methane hydrate – a major reservoir of carbon in the shallow geosphere?, Chem. Geol. 71 (1988) 41–51.
[20] S. Choi, J.H. Drese, C.W. Jones, Methane exploitation by carbon dioxide from gas hydrates—phase equilibria for CO_2-CH_4 mixed hydrate system, J. Chem. Eng. Jpn. 29 (1996) 478–483.

[21] M. Yand, Y. Song, L. Jiang, Y. Zhao, X. Ruan, Y. Zhang, S. Wang, Hydrate-based technology for CO_2 capture from fossil fuel power plants, Appl. Energy 116 (2014) 26–40.

[22] M. Ricaurte, C. Dicharry, X. Renaud, J.-P. Torré, Combination of surfactants and organic compounds for boosting CO_2 separation from natural gas by clathrate hydrate formation, Fuel 122 (2014) 206–217.

[23] B. Kvamme, A. Graue, T. Buanes, T. Kuznetsova, G. Ersland, Storage of CO_2 in natural gas hydrate reservoirs and the effect of hydrate as an extra sealing in cold aquifers, Int. J. Greenh. Gas Control 1 (2007) 236–246.

[24] V. Chihaua, S. Adams, W.F. Kuhs, Molecular dynamics simulations of properties of a (001) methane clathrate hydrate surface, Chem. Phys. 317 (2005) 208–225, https://doi.org/10.1016/j.chemphys.2005.05.024.

[25] B. Peters, N.E.R. Zimmermann, G.T. Beckham, J.W. Tester, B.J. Trout, Path sampling calculation of methane diffusivity in natural gas hydrates from a water-vacancy assisted mechanism, J. Am. Chem. Soc. 130 (2008) 17342–17350, https://doi.org/10.1021/ja802014m.

[26] N.J. English, J.S. Tse, Mechanisms for thermal conduction in methane hydrate, Phys. Rev. Lett. 103 (2009) 015901, https://doi.org/10.1103/PhysRevLett.103.015901.

[27] P.G. Debenedetti, Metastable Liquids: Concepts and Principles, Princeton University Press, 1996.

[28] D. Kashchiev, Nucleation, Butterworth-Heinemann, Oxford, UK, 2000.

[29] N. Maeda, Nucleation of Gas Hydrates, Springer Nature, Switzerland, Switzerland, 2020.

[30] D. Kashchiev, A. Firoozabadi, Driving force for crystallization of gas hydrates, J. Cryst. Growth 241 (2002) 220–230.

[31] D. Kashchiev, A. Firoozabadi, Nucleation of gas hydrates, J. Cryst. Growth 243 (2002) 476–489.

[32] L.C. Jacobson, W. Hujo, V. Molinero, Amorphous precursors in the nucleation of clathrate hydrates, J. Am. Chem. Soc. 132 (2010) 11806–11811.

[33] L.C. Jacobson, W. Hujo, V. Molinero, Nucleation pathways of clathrate hydrates: effect of guest size and solubility, J. Phys. Chem. B 114 (2010) 13796–13807.

[34] M.R. Walsh, G.T. Beckham, C.A. Koh, E.D. Sloan, D.T. Wu, A.K. Sum, Methane hydrate nucleation rates from molecular dynamics simulations: effects of aqueous methane concentration, interfacial curvature, and system size, J. Phys. Chem. C 115 (2011) 21241, https://doi.org/10.1021/jp206483q.

[35] L.C. Jacobson, V. Molinero, Can amorphous nuclei grow crystalline clathrates? The size and crystallinity of critical clathrate nuclei, J. Am. Chem. Soc. 133 (2011) 6458–6463.

[36] S. Sarupria, P.G. Debenedetti, Molecular dynamics study of carbon dioxide hydrate dissociation, J. Phys. Chem. Lett. 3 (2012) 2942–2947.

[37] B.C. Knott, V. Molinero, M.F. Doherty, B. Peters, Homogeneous nucleation of methane hydrates: unrealistic under realistic conditions, J. Am. Chem. Soc. 134 (2012) 19544–19547.

[38] S. Sarupria, P.G. Debenedetti, Homogeneous nucleation of methane hydrate in microsecond molecular dynamics simulations, J. Phys. Chem. A 115 (2011) 6102–6111.

[39] S. Liang, P.G. Kusalik, Nucleation of gas hydrates within constant energy systems, J. Phys. Chem. B 117 (2013) 1403–1410, https://doi.org/10.1021/jp308395x.

[40] B.C. Barnes, B.C. Knott, G.T. Beckham, D. Wu, A.K. Sum, Molecular dynamics study of carbon dioxide hydrate dissociation, J. Phys. Chem. B 118 (2014) 13236–13243, https://doi.org/10.1021/jp507959q.

[41] D. Yuhara, B.C. Barnes, D. Suh, B.C. knott, G.T. Beckham, K. Yasuoka, D. Wu, A.K. Sum, Nucleation rate analysis of methane hydrate from molecular dynamics simulations, Faraday Discuss. 179 (2015) 463–474, https://doi.org/10.1039/c4fd00219a.

[42] P. Warrier, M.N. Khan, V. Srivastava, C.M. Maupin, C.A. Koh, Overview: nucleation of clathrate hydrates, J. Chem. Phys. 145 (2016) 211705, https://doi.org/10.1063/1.4968590.

[43] Z. Zhang, P.G. Kusalik, G.-J. Guo, Molecular insight into the growth of hydrogen and methane binary hydrates, J. Phys. Chem. C 122 (2018) 7771–7778, https://doi.org/10.1021/acs.jpcc.8b00842.

[44] Arjun, T.A. Berendsen, P.G. Bolhuis, Unbiased atomistic insight in the competing nucleation mechanisms of methane hydrates, Proc. Natl. Acad. Sci. 116 (2019) 19305–19310, https://doi.org/10.1073/pnas.1906502116.

[45] Z. Zhang, G.-J. Guo, N. Wu, P.G. Kusalik, Molecular insights into guest and composition dependence of mixed hydrate nucleation, J. Phys. Chem. C 124 (2020) 25078–25086, https://doi.org/10.1021/acs.jpcc.0c07375.

[46] A. Arjun, P.G. Bolhuis, Rate prediction for homogeneous nucleation of methane hydrate at moderate supersaturation using transition interface sampling, J. Phys. Chem. B 124 (2020) 8099–8109, https://doi.org/10.1021/acs.jpcb.0c04582.

[47] A. Arjun, P.G. Bolhuis, Homogenous nucleation rate of CO_2 hydrates using transition interface sampling, J. Chem. Phys. 154 (2021) 164507.

[48] L. Wang, K. Hall, Z. Chang, P.G. kusalik, Mixed hydrate nucleation: molecular mechanics and cage structures, J. Phys. Chem. B 126 (2022) 7015–7026, https://doi.org/10.1021/acs.jpcb.2c03223.

[49] J. Grabowska, S. Blázquez, E. Sanz, I.M. Zerón, J. Algaba, J.M. Míguez, F.J. Blas, C. Vega, Solubility of methane in water: some useful results for hydrate nucleation, J. Phys. Chem. B 126 (2022) 8553–8570.

[50] J. Grabowska, S. Blázquez, E. Sanz, E.G. Noya, I.M. Zerón, J. Algaba, J.M. Míguez, F.J. Blas, C. Vega, Homogeneous nucleation rate of methane hydrate formation under experimental conditions from seeding simulations, J. Chem. Phys. 158 (2023) 114505.

[51] J. Algaba, I.M. Zerón, J.M. Míguez, J. Grabowska, S. Blazquez, E. Sanz, C. Vega, F.J. Blas, Solubility of carbon dioxide in water: some useful results for hydrate nucleation, J. Chem. Phys. 158 (18) (2023) 054505.

[52] L. Wang, P.G. Kusalik, Understanding why constant energy or constant temperature may affect nucleation behavior in MD simulations: a study of gas hydrate nucleation, J. Chem. Phys. 159 (2023) 184501, https://doi.org/10.1063/5.0169669.

[53] E. Sanz, J.R. Espinosa, R. Caballero-Bernal, J.L.F. Abascal, C. Valeriani, Homogeneous ice nucleation at moderate supercooling from molecular simulation, J. Am. Chem. Soc. 135 (2013) 15008–15017.

[54] J.R. Espinosa, C. Navarro, E. Sanz, C. Valeriani, C. Vega, On the time required to freeze water, J. Chem. Phys. 145 (2016) 211922.

[55] J.R. Espinosa, C. Vega, C. Valeriani, E. Sanz, Seeding approach to crystal nucleation, J. Chem. Phys. 144 (2016) 034501.

[56] G.D. Soria, J.R. Espinosa, J. Ramirez, C. Valeriani, C. Vega, E. Sanz, A simulation study of homogeneous ice nucleation in supercooled salty water, J. Chem. Phys. 148 (2018) 222811.

[57] Z.M. Aman, C.A. Koh, Interfacial phenomena in gas hydrate systems, Chem. Soc. Rev. 45 (2016) 1678–1690, https://doi.org/10.1039/C5CS00791G.

[58] A.W. Adamson, A.P. Gast, Physical Chemistry of Surfaces, John Wiley and Sons, Inc., 1997.

[59] R.D. Weir, E.Th.W. de Loos, Measurement of the Thermodynamic Properties of Multiple Phases, vol. VII, Experimental Thermodynamics, Elsevier, 2005, Ch. 15, M.J.B. Evans, Measurement of Surface and Interfacial Tensions.

[60] J.W. Gibbs, The Collected Work of J. W. Gibbs, vol. 1, Yale University Press, New Haven, 1957.

[61] N.D. Pascuale, R.L. Davidchack, Shuttleworth equation: a molecular simulations perspective, J. Chem. Phys. 153 (2020) 154705.

[62] R. Shuttleworth, The surface tension of solids, Proc. Phys. Soc. Lond. Sect. A 63 (1950) 444–457.

[63] J.W. Cahn, American Society of Metals, Metals Park, Ohio, 1979, Ch. Thermodynamics of Solid and Fluid Surfaces, pp. 17–18.

[64] T. Young, III. An essay on the cohesion of fluids, Philos. Trans. R. Soc. 95 (1805) 65–87.

[65] Y.P. Handa, D. Stupin, Thermodynamic properties and dissociation characteristics of methane and propane hydrates in 70-Å-radius silica gel pores, J. Phys. Chem. 96 (1992) 8599–8603.

[66] M.B. Clennell, M. Hovland, J.S. Booth, P. Henry, W.J. Winters, Formation of natural gas hydrates in marine sediments 1. Conceptual model of gas hydrate growth conditioned by host sediment properties, J. Geophys. Res. 104 (1999) 22,985–23,003.

[67] P. Henry, M. Thomas, M.B. Clennell, Formation of natural gas hydrates in marine sediments 2. Thermodynamic calculations of stability conditions in porous sediments, J. Geophys. Res. 104 (1999) 23,005–23,022.

[68] T. Uchida, T. Ebinuma, T. Ishizaki, Dissociation condition measurements of methane hydrate in confined small pores of porous glass, J. Phys. Chem. B 103 (1999) 3659–3662.

[69] T. Uchida, T. Ebinuma, S. Takeya, J. Nagao, H. Narita, Effects of pore sizes on dissociation temperatures and pressures of methane, carbon dioxide, and propane hydrates in porous media, J. Phys. Chem. B 106 (2002) 802–826.

[70] R. Anderson, M. Llamedo, B. Tohihi, R.W. Burgass, Characteristics of clathrate hydrate equilibria in mesopores and interpretation of experimental data, J. Phys. Chem. B 107 (2003) 3500–3506.

[71] R. Anderson, M. Llamedo, B. Tohihi, R.W. Burgass, Experimental measurement of methane and carbon dioxide clathrate hydrate equilibria in mesoporous silica, J. Phys. Chem. B 107 (2003) 3507–3514.

[72] A. Arjun, P.G. Bolhuis, Molecular understanding of homogeneous nucleation of co2 hydrates using transition path sampling, J. Phys. Chem. B 125 (2021) 338–349.

[73] A. Arjun, P.G. Bolhuis, Homogeneous nucleation of crystalline methane hydrate in molecular dynamics transition paths sampled under realistic conditions, J. Chem. Phys. 158 (2023) 044504.

[74] I.M. Zerón, J. Algaba, J.M. Míguez, J. Grabowska, S. Blazquez, E. Sanz, C. Vega, F.J. Blas, Homogeneous nucleation rate of carbon dioxide hydrate formation under experimental condition from seeding simulations, J. Chem. Phys. 162 (2025) 134708.

[75] N.D. Pasquale, J. Algaba, P.M. de Hijes, I. Sanchez-Burgos, A.R. Tejedor, S.R. Yeandel, F.J. Blas, R.L. Davidchack, J.R. Espinosa, C.L. Freeman, J.H. Harding, B.B. Laird, E. Sanz, C. Vega, L. Rovigatti, Solid-liquid interfacial free energy from computer simulations: challenges and recent advances, Chem. Rev. 125 (2025) 5003–5053.

[76] J.W. Gibbs, On the equilibrium of heterogeneous substances, Trans. Conn. Acad. Sci. 3 (1876) 108–248.

[77] M. Volmer, A. Weber, Keimbildung in übersättigten gebilden, Z. Phys. Chem. 119 (1926) 277–301.

[78] R. Becker, W. Döring, Kinetische behandlung der keimbildung in übersättigten dämpfen, Ann. Phys. 416 (1935) 719–752.

[79] K.F. Kelton, Crystal Nucleation in Liquids and Glasses, Solid State Physics, vol. 45, Elsevier, 1991, pp. 75–177.

[80] J. Algaba, E. Acuña, J.M. Míguez, B. Mendiboure, I.M. Zerón, F.J. Blas, Simulation of the carbon dioxide hydrate-water interfacial energy, J. Colloid Interface Sci. 623 (2022) 354–367, https://doi.org/10.1016/j.jcis.2022.05.029.

[81] J. Miyazaki, J.A. Barker, G.M. Pound, A new Monte Carlo method for calculating surface tension, J. Chem. Phys. 64 (1976) 3364–3369.
[82] J.Q. Broughton, G.H. Gilmer, Molecular dynamics investigation of the crystal-fluid interface. VI. Excess surface free energies of crystal-liquid systems, J. Chem. Phys. 84 (1986) 5759–5768.
[83] R.L. Davidchack, B.B. Laird, Direct calculation of the hard-sphere crystal/melt interfacial free energy, Phys. Rev. Lett. 85 (2000) 4752–4754.
[84] R.L. Davidchack, J.R. Morris, B.B. Laird, The anisotropic hard-sphere crystal-melt interfacial free energy from fluctuations, J. Chem. Phys. 125 (2006) 094710.
[85] R.L. Davidchack, Hard spheres revisited: accurate calculation of the solid–liquid interfacial free energy, J. Chem. Phys. 133 (2010) 234701.
[86] R. Handel, R.L. Davidchack, Direct calculation of solid-liquid interfacial free energy for molecular systems: TIP4P/Ice-water interface, Phys. Rev. Lett. 100 (2008) 036104.
[87] R.L. Davidchack, R. Handel, J. Anwar, A.V. Brukhno, Ice ih-water interfacial free energy of simple water models with full electrostatic interactions, J. Chem. Theory Comput. 8 (2012) 2383–2390.
[88] R.K.R. Addula, S.N. Punnathanam, Computation of solid-fluid interfacial free energy in molecular systems using thermodynamic integration, J. Chem. Phys. 153 (2020) 154504.
[89] S.R. Yeandel, C.L. Freeman, J.H. Harding, A general method for calculating solid/liquid interfacial free energies from atomistic simulations: application to $CaSO_4 \cdot x\ H_2O$, J. Chem. Phys. 157 (2022) 084117.
[90] F. Leroy, D.J. Dos Santos, F. Müller-Plathe, Interfacial excess free energies of solid-liquid interfaces by molecular dynamics simulation and thermodynamic integration, Macromol. Rapid Commun. 30 (2009) 864–870.
[91] F. Leroy, F. Müller-Plathe, Solid-liquid surface free energy of Lennard-Jones liquid on smooth and rough surfaces computed by molecular dynamics using the phantom-wall method, J. Chem. Phys. 133 (2010) 044110.
[92] F. Leroy, F. Müller-Plathe, Dry-surface simulation method for the determination of the work of adhesion of solid-liquid interfaces, Langmuir 31 (2015) 8335–8345.
[93] S. Angioletti-Uberti, M. Ceriotti, P.D. Lee, M.W. Finnis, Solid-liquid interface free energy through metadynamics simulations, Phys. Rev. B 81 (2010) 125416.
[94] A. Jabbarzadeh, Effect of molecular branching and surface wettability on solid-liquid surface tension and line-tension of liquid alkane surface nanodroplets, J. Colloid Interface Sci. 666 (2024) 355–370.
[95] I.M. Zerón, J.M. Míguez, B. Mendiboure, J. Algaba, F.J. Blas, Simulation of the CO_2 hydrate–water interfacial energy: the mold integration–guest methodology, J. Chem. Phys. 157 (2022) 134709, https://doi.org/10.1063/5.0101746.
[96] C. Romero-Guzmán, I.M. Zerón, J. Algaba, B. Mendiboure, J.M. Míguez, F.J. Blas, Effect of pressure on the carbon dioxide hydrate–water interfacial free energy along its dissociation line, J. Chem. Phys. 158 (2023) 194704.
[97] M.J. Torrejón, C. Romero-Guzmán, M.M. Piñeiro, F.J. Blas, J. Algaba, Simulation of the THF hydrate - water interfacial free energy from computer simulation, J. Chem. Phys. 161 (2024) 064701.
[98] J.R. Espinosa, C. Vega, E. Sanz, The mold integration method for the calculation of the crystal-fluid interfacial free energy from simulations, J. Chem. Phys. 141 (2014) 134709.
[99] W. Lechner, C. Dellago, Accurate determination of crystal structures based on averaged local bond order parameters, J. Chem. Phys. 129 (2008) 114707.
[100] J.R. Espinosa, C. Vega, C. Valeriani, E. Sanz, The crystal-fluid interfacial free energy and nucleation rate of NaCl from different simulation methods, J. Chem. Phys. 142 (2015) 194709.
[101] J.R. Espinosa, C. Vega, E. Sanz, Ice - water interfacial free energy for the TIP4P, TIP4P/2005, TIP4P/Ice, and mW models as obtained from the mold integration technique, J. Phys. Chem. C 120 (2016) 8068–8075.
[102] I. Zerón, C. Vega, A. Benavides, Continuous version of a square-well potential of variable range and its application in molecular dynamics simulations, Mol. Phys. 116 (2018) 3355–3365.
[103] J.L.F. Abascal, E. Sanz, R.G. Fernández, C. Vega, A potential model for the study of ices and amorphous water: TIP4P/Ice, J. Chem. Phys. 122 (2005) 234511.
[104] B. Guillot, Y. Guissani, A computer simulation study of the temperature dependence of the hydrophobic hydration, J. Chem. Phys. 99 (1993) 8075–8094, https://doi.org/10.1063/1.465634.
[105] D. Paschek, Temperature dependence of the hydrophobic hydration and interaction of simple solutes: an examination of five popular water models, J. Chem. Phys. 120 (2004) 6674–6690, https://doi.org/10.1063/1.1652015.
[106] W.L. Jorgensen, J.D. Madura, C.J. Swenson, Optimized intermolecular potential functions for liquid hydrocarbons, J. Am. Chem. Soc. 106 (1984) 6638–6646, https://doi.org/10.1021/ja00334a030.
[107] M.M. Conde, C. Vega, Determining the three-phase coexistence line in methane hydrates using computer simulations, J. Chem. Phys. 133 (2010) 064507, https://doi.org/10.1063/1.3466751.
[108] M.M. Conde, C. Vega, Note: a simple correlation to locate the three phase coexistence line in methane-hydrate simulations, J. Chem. Phys. 138 (2013) 056101, https://doi.org/10.1063/1.4790647.
[109] V.K. Michalis, J. Costandy, I.N. Tsimpanogiannis, A.K. Stubos, I.G. Economou, Prediction of the phase equilibria of methane hydrates using the direct phase coexistence methodology, J. Chem. Phys. 142 (2015) 044501, https://doi.org/10.1063/1.4905572.
[110] S. Blazquez, J. Algaba, J.M. Míguez, C. Vega, F.J. Blas, M.M. Conde, Three-phase equilibria of hydrates from computer simulation. I: finite-size effects in the methane hydrate, J. Chem. Phys. 160 (2024) 164721.
[111] A.M. Fernández-Fernández, M. Pérez-Rodríguez, A. Comesaña, M.M. Piñeiro, Three-phase equilibrium curve shift for methane hydrate in Oceanic conditions calculated from molecular dynamics simulations, J. Mol. Liq. 274 (2019) 426–433, https://doi.org/10.1016/j.molliq.2018.10.146.
[112] J. Algaba, S. Blazquez, J.M. Míguez, M.M. Conde, F.J. Blas, Three-phase equilibria of hydrates from computer simulation. III: effect of dispersive interactions in methane and carbon dioxide hydrates, J. Chem. Phys. 160 (2024) 164723.
[113] A.M. Fernández-Fernández, M.M. Conde, G. Pérez-Sánchez, M. Pérez-Rodríguez, M.M. Piñeiro, Molecular simulation of methane hydrate growth confined into a silica pore, J. Mol. Liq. 362 (2022) 119698.
[114] A.M. Fernández-Fernández, A. Bárcena, M.M. Conde, G. Pérez-Sánchez, M. Pérez-Rodríguez, M.M. Piñeiro, Modeling Oceanic sedimentary methane hydrate growth through molecular dynamics simulation, J. Chem. Phys. 160 (2024) 144107.
[115] G.M. Martin, J.I. Siepmann, Transferable potentials for phase equilibria. 1. United-atom description of n-alkanes, J. Phys. Chem. B 102 (2001) 2569–2577.
[116] D. van der Spoel, E. Lindahl, B. Hess, G. Groenhof, A.E. Mark, H.J. Berendsen, Gromacs: fast, flexible, and free, J. Comput. Chem. 26 (2005) 1701–1718.
[117] D. Frenkel, B. Smit, Understanding Molecular Simulations, 2nd ed., Academic, San Diego, 2002.
[118] E.G. Noya, C. Vega, E. de Miguel, Determination of the melting point of hard spheres from direct coexistence simulation methods, J. Chem. Phys. 128 (2008) 154507, https://doi.org/10.1063/1.2901172.
[119] D. Frenkel, Simulations: the dark side, Eur. Phys. J. Plus 128 (2013) 1–21, https://doi.org/10.1140/epjp/i2013-13010-8.
[120] J.R. Espinosa, E. Sanz, C. Valeriani, C. Vega, On fluid-solid direct coexistence simulations: the pseudo-hard sphere model, J. Chem. Phys. 139 (2013) 144502, https://doi.org/10.1063/1.4823499.
[121] M.P. Allen, D.J. Tildesley, Computer Simulation of Liquids, 2nd ed., Oxford University PressClaredon, Oxford, 2017.
[122] J. Algaba, S. Blazquez, E. Feria, J.M. Míguez, M.M. Conde, F.J. Blas, Three-phase equilibria of hydrates from computer simulation. II: finite-size effects in the carbon dioxide hydrate, J. Chem. Phys. 160 (2024) 164722.
[123] M.A. Cuendet, W.F.V. Gunsteren, On the calculation of velocity-dependent properties in molecular dynamics simulations using the leapfrog integration algorithm, J. Chem. Phys. 127 (2007) 184102.
[124] S. Nosé, A molecular dynamics method for simulations in the canonical ensemble, Mol. Phys. 52 (1984) 255–268.
[125] M. Parrinello, A. Rahman, Polymorphic transitions in single crystals: a new molecular dynamics method, J. Appl. Phys. 52 (1981) 7182–7190.
[126] U. Essmann, L. Perera, M.L. Berkowitz, T. Darden, H. Lee, L.G. Pedersen, A smooth particle mesh Ewald method, J. Chem. Phys. 103 (1995) 8577–8593.
[127] I.M. Zerón, J. Algaba, J.M. Míguez, B. Mendiboure, F.J. Blas, Rotationally invariant local bond order parameters for accurate determination of hydrate structures, Mol. Phys. 122 (21–22) (2024) e2395438.
[128] I. Sanchez-Burgos, E. Sanz, C. Vega, J.R. Espinosa, Fcc vs. hcp competition in colloidal hard-sphere nucleation: on their relative stability, interfacial free energy and nucleation rate, Phys. Chem. Chem. Phys. 23 (2021) 19611–19626, https://doi.org/10.1039/D1CP01784E.
[129] V. Molinero, E.B. Moore, Water modeled as an intermediate element between carbon and silicon, J. Phys. Chem. B 113 (2009) 4008–4016, https://doi.org/10.1021/jp805227c.
[130] L.C. Jacobson, V. Molinero, A methane-water model for coarse-grained simulations of solutions and clathrate hydrates, J. Phys. Chem. B 114 (2010) 7302–7311.
[131] Z.D.D.L.Y. Chen, R. Sun, The influence of temperature, pressure, salinity and capillary force on the formation of methane hydrate, Geosci. Front. 2 (2011) 125–135.
[132] D. Jin, J. Zhong, Reparameterization of the mw model to accurately predict the experimental phase diagram of methane hydrate, J. Chem. Phys. 161 (2024) 174504.
[133] D.B. Macleod, On a relation between surface tension and density, Trans. Faraday Soc. 19 (1923) 38–41.
[134] E.A. Guggenheim, The principle of corresponding state, J. Chem. Phys. 13 (1945) 253–261.
[135] F.J. Blas, F.J. Martínez-Ruiz, A.I. Moreno-Ventas Bravo, L.G. MacDowell, Application of the SAFT-VR density functional theory to the prediction of interfacial properties of mixtures of relevance to reservoir engineering, J. Chem. Phys. 137 (2012) 024702.
[136] J. Lee, T. Yun, J. Santamarina, C. Ruppel, Observations related to tetrahydrofuran and methane hydrates for laboratory studies of hydrate-bearing sediments, Geochem. Geophys. Geosyst. 8 (6) (2007).
[137] M. Zakrzewski, Y. Handa, Thermodynamic properties of ice and of tetrahydrofuran hydrate in confined geometries, J. Chem. Thermodyn. 25 (1993) 631–637.
[138] D. Kashchiev, G.M. van Rosmalen, Review: nucleation in solutions revisited, Cryst. Res. Technol. 38 (2003) 555–574, https://doi.org/10.1002/crat.200310070.
[139] J.W. Gibbs, On the equilibrium of heterogeneous substances, Trans. Conn. Acad. 3 (1877) 343.
[140] J. Espinosa, E. Sanz, C. Valeriani, C. Vega, Homogeneous ice nucleation evaluated for several water models, J. Chem. Phys. 141 (2014) 18C529.
[141] P.M. de Hijes, J.R. Espinosa, E. Sanz, C. Vega, Interfacial free energy of a liquid-solid interface: its change with curvature, J. Chem. Phys. 151 (2019) 144501.